LUND UNIVERSITY

Development of Photoacoustic Imaging Techniques Towards Clinical Translation

Khodaverdi, Azin

2025

Development of Photoacoustic Imaging Techniques Towards Clinical Translation

Azin Khodaverdi

Organization LUND UNIVERSITY Department of Biomedical Engineering Lund University Box 118, SE-221 00, Lund, Sweden	Document name DOCTORAL DISSERTATION
	Date of issue September 12, 2025
Author Azin Khodaverdi	**Sponsoring organization**

Title: Development of Photoacoustic Imaging Techniques Towards Clinical Translation

Abstract : This thesis encompasses an introductory part and five papers related to developing techniques and phantoms required for the further growth of photoacoustic imaging (PAI). In PAI, images are created by detecting acoustic waves followed by the absorption of laser light, enabling high spatial resolution while maintaining high optical contrast. Due to the distinct absorption patterns of various chromophores in the body, a unique photoacoustic response can be detected by changing the wavelength of the laser light. This unique photoacoustic response, called photoacoustic spectrum, is employed in a wide range of biomedical applications such as skin cancer detection and estimation of the spatial distribution of oxygen in the body. Although there have been significant advancements in the research field, this technique has not yet been adopted in healthcare, and challenges need to be addressed for its translation into clinical practice. This thesis revolves around technical advancements in PAI in different aspects that support its pathway to the clinics. Paper I introduces a tuning approach of a stable tissue-mimicking phantom (TMP) for usage in PAI studies. The results show that artists' oil-based inks dissolved in turpentine can be utilized to tune the optical absorption properties of SEBS-gel with high accuracy, creating various photoacoustic spectral shapes and amplitudes. In addition, the long-term stability investigation of these TMPs proved their effectiveness in preserving their optical properties. Paper II presents a novel automatic threshold selection (ATS) approach that can be applied to the adaptive matched filter spectral unmixing method to distinguish the target from the background. The approach was utilized on a TMP containing inclusions, and the feasibility of its use in detecting the border of malignant melanoma (MM) skin cancers was investigated. The thickness estimated by the ATS algorithm showed a root mean squared error of 0.26 mm for the phantom inclusions and 0.19 mm for the MM skin samples compared to the ground truth and histology examination. Paper III compares the performance of two previously proposed techniques to compensate for the spectral coloring. Both approaches build upon existing techniques and are modified to be adapted to the context of human in vivo and our PAI imaging system. Results showed that both methods led to similar oxygen saturation (sO$_2$) estimates and minimized the depth-dependent variations in sO$_2$ that are typically observed with linear unmixing, decreasing the gradient of saturation as a function of depth as physiologically expected in a normal situation. Paper IV introduces the center frequency (CF) spectra, the mean frequency of photoacoustic data across all wavelengths. The feasibility of using the CF spectra in separating the microspheres with various sizes and colors in a phantom study is investigated. The results showed microspheres with different pigmentation in the same size exhibited different CF spectra shapes across the utilized wavelength. Moreover, changing the size of microspheres resulted in a change in the CF offset while preserving the shape. Paper V presents the clinical application of CF spectra in PAI. A normalization was applied to remove the system dependency, defined as alpha spectra. The shape and the slope of a linear model applied to the alpha spectra were evaluated as potential biomarkers for distinguishing MM and basal cell carcinoma (BCC) from healthy tissue. The median of CF spectral slopes and spectral shapes showed significant separation, with higher alpha slope values for the tumors. In another application, changes in the alpha spectra related to variations in oxygenation of the finger during an occlusion-recovery model were investigated. Results showed significant differences in the alpha spectra, with an increase in the alpha slope observed during the occlusion phase.

Key words: Photoacoustic imaging, oxygenation measurement, skin cancer detection, tissue mimicking phantom, ultrasound imaging, center frequency, spectral coloring, spectral unmixing.

Classification system and/or index terms (if any)

Supplementary bibliographical information	Language: English
ISSN and key title	**ISBN:** 978-91-8104-630-4 (printed) 978-91-8104-631-1 (electronic)
Recipient's notes	Number of pages: 168	Price
	Security classification	

Signature   Date _____ 2025-09-12 _____

To my family

Popular science summary

Medical imaging technologies provide visual representations of the tissues and organs in the body, which are widely utilized for diagnosis and monitoring of treatment in healthcare. A recently developed non-invasive medical imaging modality, photoacoustic imaging, combines light and sound to produce high-resolution images of the structural and functional properties of the tissues. Chromophores, which are light-absorbing molecules in the body, absorb light at particular wavelengths. This creates a distinct pattern in the photoacoustic signal, which can be employed to distinguish between chromophores such as hemoglobin in the blood. This novel technique offers the potential for early detection of diseases such as cancer, as well as for monitoring tissue oxygen levels.

Skin cancer is among the most common types of cancer in Sweden, with ultra-violet light exposure being a major risk factor. The standard diagnostic procedure is a biopsy followed by a histopathological analysis, which is invasive, time-consuming, and relies on surgical excision. This makes it challenging for lesions placed on sensitive areas such as the face, head, or neck. Photoacoustic imaging has recently shown promising results as a non-invasive approach for detecting skin cancers, although further development is needed to enable its use in clinics.

Another clinically relevant application of photoacoustic imaging is the estimation of oxygen levels in tissues in the body. Measuring the spatial distribution of oxygen in the body is important for assessing organ health and evaluating cardiovascular function, a unique ability offered by photoacoustic imaging. It can also be utilized for monitoring cancer progression, especially regarding tissue hypoxia, which is defined as the deficiency of oxygen in the tissue, as well as treatment response.

Despite recent advances and the clinical approval of a few photoacoustic imaging devices, the technique is not yet widely used in clinical settings. One of the key challenges is the lack of standardized approaches to compare the quality of new imag-

ing systems, monitor performance over time, and evaluate the effectiveness of novel quantitative techniques. Tissue-mimicking phantoms are artificial materials designed to replicate the characteristics of human tissue. Tissue-mimicking phantoms with tunable properties are commonly used to validate and assess the performance of new imaging modalities and methods.

Paper I of the thesis addresses this lack of tissue-mimicking phantoms required for the development and validation of quantitative approaches in photoacoustic imaging. We developed novel tissue-mimicking phantoms with tunable optical properties by mixing copolymer-in-oil with oil-based inks. We also demonstrated their long-term stability; photoacoustic imaging measurements taken after 14 months of storage at room temperature showed consistent photoacoustic amplitude and spectrum. The material is also suitable for creating phantoms in various custom shapes, adding flexibility for research and clinical development.

Given that histology is the gold standard of skin cancer detection, developing methods that detect and delineate these tumors non-invasively is highly needed. These methods can act as a guide for the physician to detect cancer lesions that may not be visible during the examination or surgery. In **paper II**, an automatic method capable of separating malignant melanoma tumors from healthy tissues was developed, enabling the estimation of tumor boundaries, including the thickness and width. In **paper IV**, a novel technique based on the frequency characteristics of photoacoustic data, called center frequency analysis, showed the feasibility of tissue characterization in a phantom study. The extent of this method was used in **paper V** and demonstrated the potential to detect both malignant melanoma and basal cell carcinoma from healthy tissues.

Photoacoustic imaging provides a deeper spatial distribution of oxygen than traditional optical techniques in the body. However, the accuracy of these measurements decreases with depth due to wavelength-dependent light attenuation, which alters the spectral pattern and reduces the accuracy of oxygen estimation. In **paper III**, we adapted two correction methods to our photoacoustic imaging system to improve oxygen estimation in deeper tissues under human *in vivo* conditions, helping to overcome the common challenge of wavelength-dependent light attenuation. In addition, in **paper V**, the center frequency analysis was used to monitor changes in the oxygenation during occlusion-recovery of the finger.

In summary, the five papers included in this thesis contribute to improving its progress toward clinical translation by suggesting a novel phantom material, improving tumor boundary delineation, making two spectral colouring techniques ready for *in vivo* measurements on humans, as well as suggesting a novel tissue characterisation method using center frequency analysis of the photoacoustic signal.

Abstract

This thesis encompasses an introductory part and five papers related to developing techniques and phantoms required for the further growth of photoacoustic imaging (PAI). In PAI, images are created by detecting acoustic waves followed by the absorption of laser light, enabling high spatial resolution while maintaining high optical contrast. Due to the distinct absorption patterns of various chromophores in the body, a unique photoacoustic response can be detected by changing the wavelength of the laser light. This unique photoacoustic response, called photoacoustic spectrum, is employed in a wide range of biomedical applications such as skin cancer detection and estimation of the spatial distribution of oxygen in the body. Although there have been significant advancements in the research field, this technique has not yet been adopted in healthcare, and challenges need to be addressed for its translation into clinical practice. This thesis revolves around technical advancements in PAI in different aspects that support its pathway to the clinics.

Paper I introduces a tuning approach of a stable tissue-mimicking phantom (TMP) for usage in PAI studies. The results show that artists' oil-based inks dissolved in turpentine can be utilized to tune the optical absorption properties of SEBS-gel with high accuracy, creating various photoacoustic spectral shapes and amplitudes. In addition, the long-term stability investigation of these TMPs proved their effectiveness in preserving their optical properties.

Paper II presents a novel automatic threshold selection (ATS) approach that can be applied to the adaptive matched filter spectral unmixing method to distinguish the target from the background. The approach was utilized on a TMP containing inclusions, and the feasibility of its use in detecting the border of malignant melanoma (MM) skin cancers was investigated. The thickness estimated by the ATS algorithm showed a root mean squared error of 0.26 mm for the phantom inclusions and 0.19 mm for the MM skin samples compared to the ground truth and histology examination.

Paper III compares the performance of two previously proposed techniques to compensate for the spectral coloring. Both approaches build upon existing techniques and are modified to be adapted to the context of human *in vivo* and our PAI imaging system. Results showed that both methods led to similar oxygen saturation (sO_2) estimates and minimized the depth-dependent variations in sO_2 that are typically observed with linear unmixing, decreasing the gradient of saturation as a function of depth as physiologically expected in a normal situation.

Paper IV introduces the center frequency (CF) spectra, the mean frequency of photoacoustic data across all wavelengths. The feasibility of using the CF spectra in separating the microspheres with various sizes and colors in a phantom study is investigated. The results showed microspheres with different pigmentation in the same size exhibited different CF spectra shapes across the utilized wavelength. Moreover, changing the size of microspheres resulted in a change in the CF offset while preserving the shape.

Paper V presents the clinical application of CF spectra in PAI. A normalization was applied to remove the system dependency, defined as alpha spectra. The shape and the slope of a linear model applied to the alpha spectra were evaluated as potential biomarkers for distinguishing MM and basal cell carcinoma (BCC) from healthy tissue. The median of CF spectral slopes and spectral shapes showed significant separation, with higher alpha slope values for the tumors. In another application, changes in the alpha spectra related to variations in oxygenation of the finger during an occlusion-recovery model were investigated. Results showed significant differences in the alpha spectra, with an increase in the alpha slope observed during the occlusion phase.

List of publications

Papers

I. **Optical Tuning of Copolymer-in-oil Tissue-mimicking Materials for Multispectral Photoacoustic Imaging.**
Azin Khodaverdi, Magnus Cinthio, Esbjörn Reistad, Tobias Erlöv, Malin Malmsjö, Sophia Zackrisson, Nina Reistad
Published in: Biomedical Physics & Engineering Express, vol. 10, 055009, 2024

Author's contribution: Planning and carrying out the acoustic and photoacoustic experiment, data analysis of acoustic and photoacoustic data, writing the first draft, and revising.

II. **Automatic Threshold Selection Algorithm to Distinguish a Tissue Chromophore from the Background in Photoacoustic Imaging.**
Azin Khodaverdi, Tobias Erlöv, Jenny Hult, Nina Reistad, Agnes Pekar–Lukacs, John Albinsson, Aboma Merdasa, Rafi Sheikh, Malin Malmsjö, Magnus Cinthio
Published in: Biomedical Optics Express, vol. 12, 3836-3850, 2021

Author's contribution: Planning the study, phantom manufacturing, performing the phantom experiment, method development, analysis of phantom and clinical data, writing the first draft, and revising.

III. **Two Photoacoustic Spectral Coloring Compensation Techniques Adapted to the Context of Human In-vivo Oxygenation Measurements.**
Azin Khodaverdi, Baptiste Jayet, Tobias Erlöv, John Albinsson, Aboma Merdasa, Nils Gustafsson, Rafi Sheikh, Malin Malmsjö, Stefan Andersson-Engels, Magnus Cinthio
Published in: Biomedical Optics Express, vol. 16, 2217-2231, 2025

* Azin Khodaverdi and Baptiste Jayet share first authorship

Author's contribution: Planning the study, performing the clinical data experiment and data collection, developing method A and analysis related, writing half of the first draft, and revising.

IV.   **The Feasibility of Using Center Frequency Spectra in Photoacoustic Imaging for Tissue Characterization.**
Azin Khodaverdi, Malin Larsson, Klara Wahldén, John Albinsson, Malin Malmsjö, Nina Reistad, Tobias Erlöv, Magnus Cinthio
Published in: 2023 IEEE International Ultrasonics Symposium (IUS), 1-3, 2023

Author's contribution: Planning the study, performing the photoacoustic experiment and data collection, method development, analysis of data, writing the first draft of the proceeding, and revising.

V.   **Center Frequency Spectrum Analysis in Photoacoustic Imaging for Clinical Tissue Characterization.**
Azin Khodaverdi, Tobias Erlöv, Magne Stridh, Marcus Tegner, John Albinsson, Maria Evertsson, Malin Malmsjö, Magnus Cinthio
In Manuscript

Author's contribution: Planning the study, performing the oxygenation experiment and data collection, method development, analysis of all clinical data, writing the first draft, and revising.

Papers not included in this thesis

VI. **Comparison of Photoacoustic Imaging and Histopathological Examination in Determining the Dimensions of 52 Human Melanomas and Nevi Ex vivo.**
Jenny Hult, Aboma Merdasa, Agnes Pekar-Lukacs, Magne Tordengren Stridh, **Azin Khodaverdi**, John Albinsson, Bodil Gesslein, Ulf Dahlstrand, Linn Engqvist, Yousef Hamid, Douglas Larsson Albèr, Bertil Persson, Tobias Erlöv, Rafi Sheikh, Magnus Cinthio, Malin Malmsjö
Published in: Biomedical Optics Express, vol. 12, 4097-4114, 2021

VII. **Ultrasonographic Measurement of Common Carotid Artery Wall Pulse Dynamics and Longitudinal Motion–Method Validation and a Novel Parameter Ratio.**
Artturi Petäjä, Yuxiang Zhu, **Azin Khodaverdi**, Tobias Erlöv, Åsa Rydén Ahlgren, Magnus Cinthio
Published in: Ultrasound in Medicine and Biology, vol. 51, 559-567, 2025

Acknowledgments

I would like to express my gratitude to many people who made my Ph.D. journey possible and made it a joyful experience over the years.

First and foremost, I would like to express my deep gratitude to my supervisor, *Magnus Cinthio*, who walked me through this journey. Magnus, your invaluable help, support, and encouragement provided me with the opportunities for learning and growth. You listened patiently, trusted me, and guided me during this time. Your knowledge, kindness, and unwavering support made my Ph.D. journey truly meaningful. I will always remain grateful and hope to stay in contact in the future.

I would like to extend my heartfelt thanks to my co-supervisor, *Tobias Erlöv*, for invaluable support from the very beginning of this journey to the very end. Your technical expertise and willingness to engage with even the smallest of challenges meant a great deal to me and played a crucial role in making this work possible. I have learned so much from you and will always appreciate your time. A special thanks goes to my co-supervisor, *Malin Malmsjö*. You taught me so much during this time, and I am sincerely grateful for the many in-depth clinical discussions we shared. I have always felt proud to be part of your group and to have had the opportunity to learn from you, both professionally and personally. I would also like to thank my co-supervisor, *Nina Reistad*, for enriching conversations on optics and for the great moments we spent discussing various topics. Your insights and thoughtful perspectives were invaluable, and I truly learned a lot from our discussions. Finally, I would like to thank my co-supervisor, *Maria Evertsson*, who joined the project toward the end. Sharing an office with you provided the opportunity for many meaningful exchanges. Thank you for your kindness, support, and friendship throughout this journey.

I would like to thank the current and former members of the Ultrasound group. *Jules*, I truly appreciate your friendship in the department, at conferences, and beyond. Thanks to *Tomas*, *Artturi*, and *Monica* for all the time spent and the discussions we

had together. A special thanks to *John*, who was always present and helping from the first moment I joined until the end. I enjoyed our discussions in the lab and have learned a lot from you. This journey was not possible without the help and support of my group at the eye clinic, *Aboma*, *Alice*, *Jenny*, *Magne*, *Marcus*, *Nils*, and *Rafi*. A special thanks to our collaborators, *Baptiste* and *Stefan*, at Cork University, whose valuable contributions and insights enriched this work and made our collaboration both productive and enjoyable.

I would like to extend my thanks to everyone at the *Department of Biomedical Engineering* for making these years such a nice time for me. A special thanks to *Mostafa* for being a great friend and colleague from the beginning of my time in Lund, and *Harry* for all your help, especially when we first entered Sweden. Thank you, *Ulrika*, *Ammi*, and *Désirée*, for your help with administrative work and for always supporting me with kindness. A special thanks to *Leif* and *Martin* for our discussions in the corridor on various topics. Thank you, *Axel*, for always helping me with different problems along the way. I want to thank my friends at the BME, *Enrico*, *Livia*, *Felix*, *Franzi*, *Jonathan*, and *Mahdi*, for all our nice moments during lunches and fika times.

I am deeply grateful for the many friendships I built while in Lund. *Hedieh* and *Peyman*, *Shaghayegh* and *Ali N*, *Shiva* and *Ashkan*, and *Negin* and *Saeed*, thank you for all the wonderful moments we shared from the very beginning: during our trips, lunches, weekends together, and up to today. Your presence made my time in Lund truly special and filled it with memories I will always hold dear.

It all started with a Swedish class, but a true friendship found its way and continued to grow. Thanks to *Negar*, *Nicholas*, *Pegah*, and *Amin* for all the laughs and joyful times that brightened this journey and my time in Lund. To *Nika* and *Ali H*, thank you for all your support over the years, and for your warm hospitality and kindness in so often welcoming us into your home. Spending time in Lund would not have been as enjoyable without *Sima*, *Hassan*, *Maryam*, *Natalie*, *Najmeh*, and *Vessal*. Thank you for the great moments we had together.

I cannot imagine having come this far without the unconditional love of my *parents* throughout these years. My visits to Iran were always a source of renewed energy, filled with your love, care, and encouragement. Thanks to my wonderful *sisters*, your love for your little sister has always felt like a piece of heaven. I'm also grateful to my *brothers-in-law* and my sweet little *nephews* and *niece*, whose warmth and joy made our time together truly unforgettable. To my *husband's family*, thank you for your support over the years and for the wonderful moments we've shared.

And last but certainly not least, I want to express my deepest gratitude to my beloved husband, *Hesam*. I had the privilege of sharing not only life but also the early stages of this journey with you as a colleague. Your unwavering love, encouragement, and belief in me have meant more than words can express. Thanks for standing by my side in work, in life, and in every challenge along the way. Finally, to the little one

on the way, you have already brought so much hope and joy. I can't wait to meet you.

Azin
Lund, August 2025

Author's declaration of generative AI assistance

In the preparation of this thesis, OpenAI's ChatGPT and GrammarlyGO were used to assist the writing process. All outputs generated by these tools were critically reviewed and edited by the author, who is fully accountable for the content and integrity of this work.

List of abbreviations

3D three-dimensional

AMF adaptive matched filter

ATS automatic threshold selection

BCC basal cell carcinoma

CF center frequency

CSCC cutaneous squamous cell carcinoma

DRS diffuse reflectance spectroscopy

HbO$_2$ oxyhemoglobin

HbR deoxyhemogloin

HSI hyperspectral imaging

MM malignant melanoma

MRI magnetic resonance imaging

NIRS near-infrared spectroscopy

OCT optical coherence tomography

PA photoacoustic

PAI photoacoustic imaging

PET positron emission tomography

RF radio frequency

SEBS styrene-ethylene/butylene-styrene

SPECT single-photon emission computed tomography

sO$_2$ oxygen saturation

TMM tissue-mimicking material

TMP tisue-mimicking phantom

UV ultraviolet

Contents

Part I

Introduction

Chapter 1

Introduction

1.1 Background

Photoacoustic imaging (PAI), a novel imaging technique capable of providing molecular information with the high spatial resolution of ultrasound, has attracted significant interest in recent years [1]. This hybrid imaging technique combines ultrasound and optical imaging. Ultrasound is a real-time, cost-effective, non-ionizing, and clinically available technique for visualizing the body's structures. In contrast, optical imaging offers high molecular optical contrast but is limited by high light scattering, which leads to reduced resolution and restricted penetration depth [2]. Combining these two modalities presents an opportunity to achieve high optical contrast at greater depths and with high spatial resolution of ultrasound, potentially leading to the discovery of new biomarkers that can be utilized in clinical diagnosis [3]. This modality enables visualization of endogenous chromophores in the body, such as melanin, hemoglobin, fat, and water, making it valuable for a wide range of clinical applications. These applications encompass cancer diagnosis, dermatologic imaging, neuroimaging, vascular and cardiovascular imaging, and monitoring the spatial map of oxygen in the body [4].

1.2 Motivation and aims

PAI is a unique imaging modality with many potential clinical applications. Despite the advancement, PAI is a complex technology to be translated into the clinic [5]. So far, the majority of PAI applications are focused on preclinical and clinical research, and the clinical breakthrough has not yet occurred. The need for further technical developments regarding the PAI is recognized. Our group has been focusing on research related to clinical translation of PAI system with access to human tissue samples

ex-vivo and *in-vivo*. The projects presented in this thesis were defined to support this translation with the technical developments required to promote future patient outcomes with access to human clinical data.

1.3 Thesis outline

The projects in this thesis are closely related to the developments of approaches needed for clinical translation of PAI. This thesis consists of two parts: the first part provides an introductory overview of the projects, along with a review of state-of-the-art literature related, and the second part comprises the five research papers. The introductory part begins with presenting the history and fundamental principles of PAI, along with a comparison to other medical imaging modalities, presented in chapter 2. Chapter 3 outlines the clinical motivation for PAI in this thesis, which includes oxygenation measurements and skin cancer detection. Chapter 4 provides a brief introduction to the tisue-mimicking phantoms (TMPs) usage in PAI and various kinds of TMPs manufactured and used in this thesis. Chapter 5 provides an overview of processing analysis used in PAI, including spectral unmixing, spectral coloring, and frequency analysis. Chapter 6 presents a short summary of the papers included in this thesis. Finally, chapter 7 presents the conclusion and outlook of this work.

1.4 Ethical considerations

The work included in this thesis was carried out with approval from the Swedish Ethical Review Authority, which complies with the World Medical Association's Declaration of Helsinki for medical research concerning human subjects, as updated in 2013. In this thesis work, we have used human clinical data *ex vivo* and *in vivo*. All subjects voluntarily agreed to participate in these studies and provided informed consent. All data were stored anonymously. The *in vivo* studies included in this thesis were designed to be non-invasive. The energy output of the ultrasound and laser as well as electrical safety have been taken into consideration. The staff handling the data received necessary training, including laser safety procedures.

Chapter 2 ———————

Photoacoustic imaging

2.1 History and fundamental principles

Photoacoustic (PA) effect was first discovered by Alexander Graham Bell in 1880 when he found that sound waves can be generated by exposing substances to interrupting light beams [6], [7]. However, the use of the PA effect in the biomedical field started later with the innovation of laser light sources and ultrasound transducers. PA was initially used in gas spectroscopy, where the term 'optical-acoustic' was introduced [8], and then its theory continued to be developed for condensed solid materials and its application in biomedicine [9], [10].

PAI is an emerging non-invasive imaging modality that combines ultrasound and optical imaging benefits. In PAI, nanosecond laser pulses illuminate the tissue. Light absorption creates heat and a localized temperature increase, followed by a thermoelastic expansion that generates acoustic waves that propagate through the tissue. Using an ultrasound transducer, the location of the local absorber can be detected and processed to create high-resolution images [1], [11] (see Fig. 2.1). The combination of the high contrast of optical imaging in combination with the high penetration depth of ultrasound imaging enabled PAI to be used in a wide range of clinical applications [12], [13]. PAI grants access to novel imaging biomarkers indicative of diseases that were not possible with pure optical or ultrasound imaging [14].

The amplitude of the PA signal is highly dependent on the distribution of absorbed optical energy [1], [15], which is mainly dependent on the optical absorption properties of the tissue and the amount of light that has reached the tissue. In PAI, various wavelengths of laser light are being used based on the unique absorption spectra of chromophores such as hemoglobin, melanin, lipid, and water (see Fig. 2.2). PAI can be performed in the wavelength range of 650-1000 nm (NIR-I) and 1000-1700 nm (NIR-II) [16], [17]. Due to the unique absorption of these
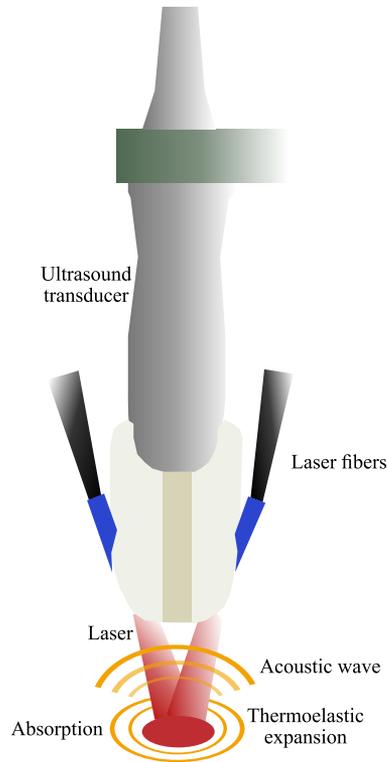
Figure 2.1: Illustration of PAI system. The tissue is illuminated with laser light, and the absorption of light creates a localized temperature rise. This leads to thermoelastic expansion, generating acoustic waves that are detectable by an ultrasound transducer, and undergoes image processing to create PA images.

chromophores in the body, multi-wavelength excitation allows selective imaging of specific chromophores. For instance, oxyhemoglobin (hemoglobin bound to oxygen) and deoxyhemoglobin (hemoglobin not bound to oxygen) exhibit distinct absorption at approximately 850 nm and 760 nm, respectively, enabling the assessment of blood oxygenation levels. Similarly, melanin absorbs strongly in the visible and NIR-I, while lipids, water, and collagen have higher absorption in the NIR-II, allowing for targeted imaging of the chromophore of interest [1]. This has enabled PAI to provide functional imaging to map the concentration and spatial distribution of the selective chromophore of interest in the body. In the studies included in this thesis, we used a wavelength range of 680-970 nm, which is non-ionizing and is well suited for deep tissue imaging due to low water absorption and tissue scattering [1].
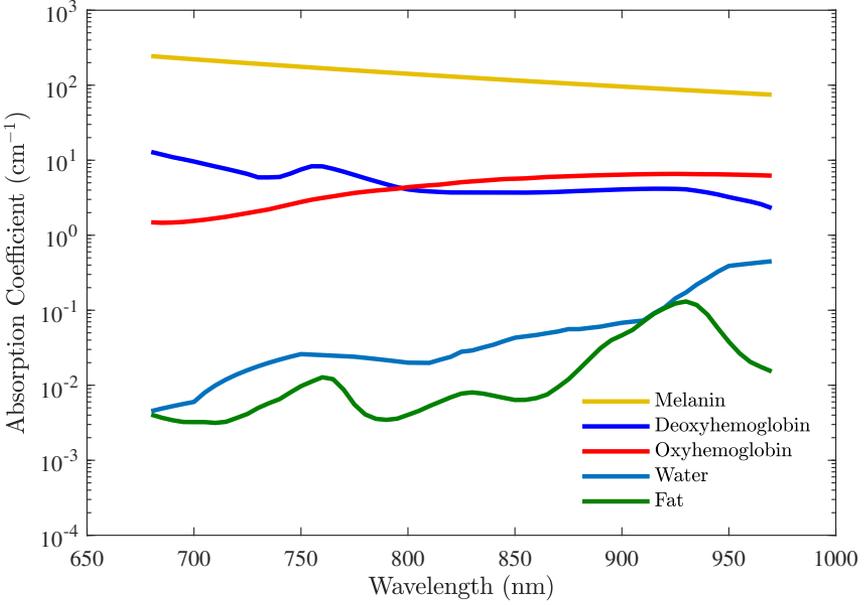
Figure 2.2: Absorption coefficients of biological chromophores in the wavelength range of 680–970 nm for melanin, deoxyhemoglobin, oxyhemoglobin, water, and fat. Different chromophores exhibit unique absorption spectra, which enables multi-wavelength photoacoustic imaging for tissue characterization. Reproduced from data in [18].

The local pressure rise in PAI can be written as:

$$p_0 = \Gamma \Phi \mu_a \tag{2.1}$$

where p_0 is the generated photoacoustic pressure, Γ the Grüneisen parameter (depends on the efficiency of heat conversion to pressure waves), μ_a the optical absorption coefficient, and Φ is the light fluence, the energy of laser per unit area [19]. By substituting μ_a with a product of molar absorption coefficient spectra $\alpha_i(\lambda)$ and their concentration $C_i(x)$ for K chromophores present in the tissue, the formula can be written as :

$$p_0 = \Gamma \Phi(r, \lambda, \mu_a, \mu_s) \sum_{i=1}^{K} \alpha_i(\lambda) C_i(r) \tag{2.2}$$

where the fluence component depends on the position r, the laser wavelength λ, the optical absorption coefficient μ_a, and the scattering coefficient μ_s [11], [20].

In PAI, multispectral PA images are acquired by varying the wavelengths of the illuminating light. PA spectrum is generated by calculating the PA amplitude as a function of wavelength, as shown in Fig. 2.3. PA spectrum conveys valuable information regarding the optical absorption of chromophores present in the tissue. Applying spectral unmixing techniques (detailed in chapter 5) can be used to estimate the spatial map of various chromophores in the tissue.
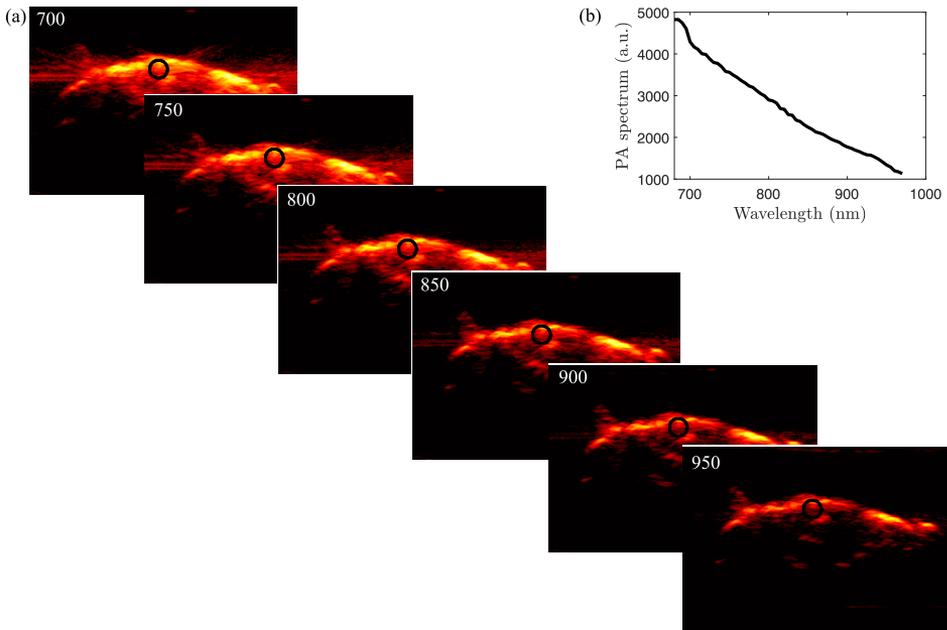
Figure 2.3: (a) PA images of a tissue sample at 700, 750, 800, 850, 900, and 950 nm, with the selected region of interest (ROI) indicated. (b) PA spectrum computed by averaging the PA amplitude within the selected ROI across all wavelengths.

2.2   Photoacoustic imaging system

The PAI system and the measurement setup used in this thesis were based on the Vevo LAZR-X imaging platform (FUJIFILM VisualSonics Inc., Toronto, ON, Canada). The system uses two laser beams on each side of the ultrasound transducer to illuminate the object of interest with nanosecond laser pulses and a frequency of 20 Hz. PA data were acquired using the VisualSonics MX250 linear array transducer, with an ultrasound center frequency of 21 MHz and frequency range of 15–30 MHz. The axial and lateral resolutions of the transducer are 75 μm and 165 μm, respectively.

In this thesis, high-frequency ultrasound detection was used, enabling the capture of higher-frequency components that usually originate from small targets [21]. Three-dimensional (3D) imaging was achieved using an adjustable arm driven by a stepper motor. Calibration of laser energy was performed at the beginning of each measurement by using an energy meter, and the PA signal at each wavelength was corrected for the differences in the laser energy at different wavelengths. The data were recorded in the wavelength range of 680 nm to 970 nm in 5 nm increments.

A shielding box was used to image the tissue-mimicking phantoms and *ex vivo* tissues. In the *in vivo* measurements, laser goggles were used for eye protection. A 10 mm aquaflex ultrasound gel pad (Parker Laboratories Inc.) was placed between the ultrasound transducer and the object of interest to have the laser focus on the surface of the phantom or tissue and limit the maximum permissible exposure of the laser radiation on the skin. The laser exposure has been measured in a previous study by our group and has been less than $20 \, \text{mJ/cm}^2$, which is the recommendation level for the wavelength range of 400- 700 nm [22].

2.3   Comparison to other imaging modalities

PAI is a rapidly evolving hybrid imaging modality that uses non-ionizing laser pulses to obtain tissue characteristics unlike the ionizing imaging modalities such as X-ray. Positron emission tomography (PET) and single-photon emission computed tomography (SPECT) are highly sensitive imaging modalities capable of providing molecular and metabolic information. However, their limited spatial resolution and reliance on ionizing radiation restrict their long-term usage in clinical applications [23]. Magnetic resonance imaging (MRI) is a non-ionizing, high-resolution imaging modality, but it is slow and expensive [24]. Optical imaging, including diffuse reflectance spectroscopy (DRS), optical coherence tomography (OCT), and hyperspectral imaging (HSI), offers high optical contrast and the ability to monitor molecular properties [25], [26]. Still, their application is limited to a superficial depth due to light scattering. Ultrasound imaging is a real-time, low-cost imaging technique with less scattering compared to optical imaging. So, combining optical and ultrasound, PAI combines the high contrast of optical imaging with the high spatial resolution of ultrasound imaging in the order of cm compared to mm [27]. This imaging technique can be combined with ultrasound or used separately and is capable of creating real-time images.

2.4   Artifacts in photoacoustic imaging

In PAI, the acoustic signal is generated from the absorption of light, and multiple artifacts can arise [28]. One of the artifacts is fluence decay, especially due to a strong absorber. The nonhomogeneous laser energy at various wavelengths and depths, referred to as spectral coloring [11], could cause uncertainty in the quantitative analysis, which will be detailed in chapter 5. In most PA processing, a homogeneous PA efficiency is assumed. However, the Grüneisen parameter can be temperature-dependent [29], [30]. On the acoustic part, various tissues inside the body have different speeds of sound and acoustic attenuation. Assuming homogeneous acoustic properties will also create sources of artifacts in the PA images, causing wrong absorber location detection or blurring of the image [31], [32]. Using dual PA-Ultrasound systems can aid in identifying some artifacts by using the ultrasound images from the same target region. In addition, the transducer characteristics, such as the limited frequency bandwidth, create artifacts in the image.

2.5   Clinical translation of photoacoustic imaging

An important step in the clinical translation of PAI has happened with some commercial PAI modalities being approved for clinical usage with a CE mark [33], [34]. MSOT Acuity Echo system (iThera Medical GmbH, Munich, Germany) has been CE-certified for handled PA and ultrasound imaging since 2021. The Imagio breast imaging system (Seno Medical Instruments, San Antonio, USA), which contains PA and ultrasound, gained the FDA's approval in 2021 for breast imaging applications. This clearly shows the potential of PAI in medical applications. The research in this thesis has been performed with a preclinical imaging system (FUJIFILM VisualSonics Inc., Toronto, ON, Canada) with approval from the Ethics Committee of Lund University, Sweden, on *ex vivo* and *in vivo* human data.

Despite the approval of these imaging systems and increasing research in the field, PAI has not been integrated into healthcare, and most of its usage focuses on preclinical and clinical research. Hardware improvement and more advanced image processing techniques are required to integrate this novel modality into clinics [5], [35]. As an example, biological chromophores exhibit a broad frequency range, so the ultrasound transducers need to have a wide bandwidth to capture most of the signal [36]. Furthermore, integrating the laser systems with the ultrasound modalities requires routine laser checkups, a special operating room, and additional training to ensure the safety, high energy output and wavelength sensitivity [5]. Spectral coloring is another challenge, arising from heterogeneous light distribution in the body, which makes accurate estimation of the chromophore's contribution difficult [37]. Additionally,

since PAI utilizes multiple wavelengths, motion compensation techniques are important to achieve a better signal-to-noise ratio [38]. Moreover, the impact of skin color on changing the received signal is another issue in quantitative PAI that needs to be addressed [39]. To ensure the reproducibility of PAI results and validate the novel methods, test objects like phantoms that are stable and keep their characteristics for a long time are needed [40]. The projects in this thesis were defined to address some of these challenges and help move PAI one step closer to clinical use with access to human clinical data.

Chapter 3
Clinical motivation

3.1   Oxygenation measurement

Measuring oxygen supply in the body is a crucial indicator of the health of various organs. Monitoring oxygen levels can be used to assess the function of the cardiovascular system [41] and is essential for patient monitoring during surgical procedures [42]. Furthermore, oxygen deficiency in various organs can be associated with organ failure or cancer progression. In addition, tumor hypoxia is a parameter that can be utilized to track the cancer treatment and tumor aggressiveness in the body [43], [44]. One of the key parameters that can be used to estimate the level of oxygen in the body is oxygen saturation (sO_2), the ratio of oxyhemoglobin (HbO_2) to total hemoglobin (HbO_2 and deoxyhemogloin (HbR)) in the body [23] as below:

$$sO_2 = \frac{[HbO_2]}{[HbR] + [HbO_2]} \tag{3.1}$$

where $[HbO_2]$ and $[HbR]$ are the concentrations of HbO_2 and HbR, respectively. Several techniques are available to measure sO_2 in the body. Among these, pulse oximetry is one of the most commonly used in healthcare. The two wavelengths utilized in this technique are usually 660 nm and 940 nm. However, it only estimates arterial oxygen level and lacks spatial resolution [45]. Furthermore, the accuracy of oxygen measurements obtained by pulse oximetry is limited by its calibration range. It has been shown to overestimate oxygen levels in individuals with darker skin tones, particularly at lower oxygen levels [46].

Various optical techniques, such as near-infrared spectroscopy (NIRS) and DRS, can be utilized to estimate tissue oxygen level (sO_2). NIRS, for instance, employs near-infrared light to illuminate biological tissues and measures the absorption and scattering of light to calculate oxygenation levels [47]. Similarly, DRS analyzes the

reflected light in the visible to near-infrared wavelength range to assess tissue oxygenation based on absorption characteristics [48]. These pure optical techniques are used in superficial depth and are inherently limited in penetration depth and spatial resolution due to the significant scattering of light in biological tissues, restricting their capability to investigate deeper tissue in the body and provide a spatial map of tissue oxygenation.

In contrast, PAI overcomes this depth resolution and estimates the spatial map of sO_2 in the body with high optical contrast and deeper than common optical techniques by transforming the light to sound. The feasibility of estimating depth-resolved sO_2 maps using PAI in several pre-clinical studies has been shown. PAI has shown promise in monitoring ischemia-reperfusion model in humans by providing depth-resolved sO_2 maps during induced vascular occlusion in the finger [49]. It has been used in oncology applications to assess tumor hypoxia [50], giving insight into cancer progression, as well as to estimate sO_2 to monitor tumor vessel disruption and cancer treatment [51]. The use of two wavelengths, selected to exploit the differential absorption of endogenous chromophores such as HbO_2 and HbR, is typically sufficient for estimating sO_2. However, employing additional wavelengths allows for the inclusion of other chromophores, depending on the application, such as melanin, fat, water, and collagen. This multi-wavelength approach enables more accurate sO_2 estimation by accounting for complex tissue compositions [52] and provides greater flexibility in post-processing analysis to select the best wavelength subset. In papers III and V, the wavelengths of 680 nm to 970 nm, in steps of 5 nm, were used for oxygenation measurements in the finger data. The setup used for measuring sO_2 in the finger is shown in Fig. 3.1, along with an example of the sO_2 map estimated using linear unmixing.

3.1.1   Occlusion versus recovery

PAI can be utilized to monitor changes in the oxygenation with spatial resolution, for example, during the vascular occlusion or adrenaline injection [49], [53]. A pressure cuff can be utilized to change the oxygenation levels in the finger. A pressure cuff exceeding 220 mmHg causes hypoxia, and releasing it leads to a recovery phase. Figure 3.2 shows a setup where a pressure cuff has been used to lower the oxygenation in the finger, together with the spatial map of sO_2 in three phases of baseline, occlusion, and recovery. Linear spectral unmixing was applied to the averaged PA signal. The original spectrum, fitted spectrum, and corresponding contribution spectra for each chromophore are displayed (linear spectral unmixing is detailed in chapter 5). In paper V, this model has been used to change the oxygenation in the finger.
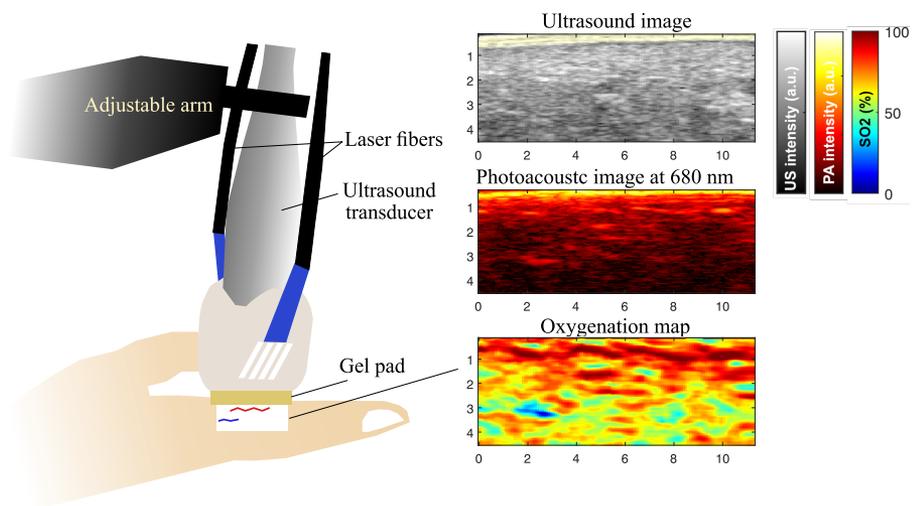
Figure 3.1: Illustration of the PAI system for oxygenation measurement in finger. The ultrasound, PA image at 680 nm, and the oxygenation map of the finger estimated using linear unmixing are shown.
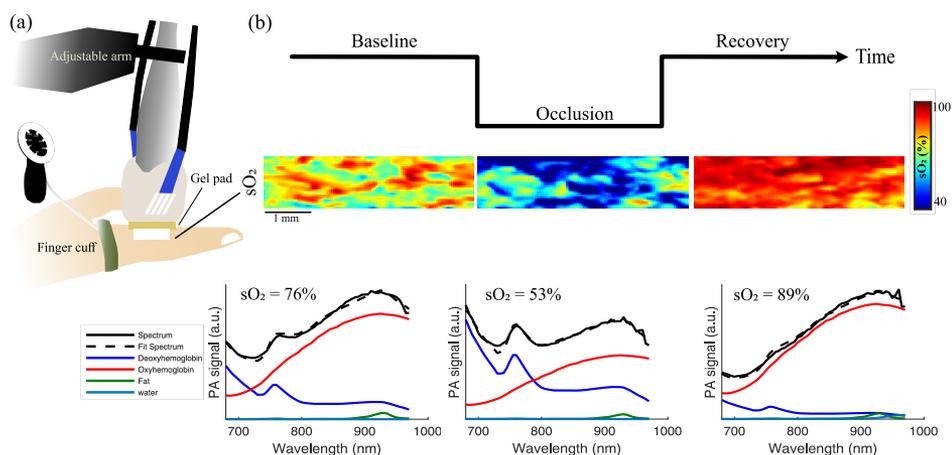
Figure 3.2: (a) Illustration of the PAI system used for finger occlusion measurements. (b) Baseline, occlusion, and recovery phases are shown with spatial maps of sO_2. Linear spectral unmixing was applied to the averaged PA signal, where the original spectrum, fitted spectrum, and the contribution of each chromophore are shown.

3.2   Skin cancer detection and delineation

3.2.1   Skin anatomy

Skin, as the outer layer of the body, is responsible for certain essential functions, including working as a waterproof protective shield, protection against infections and ultraviolet (UV) light, acting as a storage for water and fat, and regulating the temperature of our body [54]. It consists of three layers: the epidermis, dermis, and hypodermis. The epidermis is the external layer of human skin and is primarily composed of keratinocytes and melanocytes cell types. Keratinocytes produce keratin, which protects the skin from outer damage, while melanocytes create melanin, the pigment that determines skin color and protects against UV radiation. This layer contains no blood vessels, and its thickness varies between approximately 0.02 mm on the face to 0.5 mm on the fingertips [55]. The second layer of skin is the dermis, with a thickness of approximately 1 mm, including collagen fibers, blood vessels, muscles, and nerves [56]. The third layer of skin is the hypodermis, which contains subcutaneous fat, blood vessels, and connective tissue [57].

3.2.2   Skin cancer

Skin cancers are cancer cells that develop from the skin layer. One of the main risk factors is exposure to the sun's UV radiation. The three primary skin cancers include malignant melanoma (MM), basal cell carcinoma (BCC), and cutaneous squamous cell carcinoma (CSCC) [58]. The gold standard method for diagnosing skin cancer is a biopsy, followed by a histopathological examination. After surgical excision, the tumor is sent for examination, where a pathologist evaluates its type, thickness, width, and margins. The Breslow is a parameter defining the thickness of the tumor, correlated with a greater risk of metastases [59]. Given its invasive nature, time consumption, reliance on excised tissue analysis, and the sensitive locations of most skin cancers on the face and head, there is a great need for non-invasive techniques for early detection of these tumors rather than biopsy. In addition, the surgery may need to be repeated if the tumor cells are found on excision margins, which is a high-cost and time-consuming procedure [60]. Several non-invasive techniques such as dermoscopy, OCT, DRS, fluorescence spectroscopy, and high-frequency ultrasound have shown promise. However, optical techniques are limited by their penetration depth, and high-frequency ultrasound lacks molecular and functional information. PAI has recently demonstrated significant effectiveness in non-invasive cancer detection [61], [62]. In this thesis, the potential of PAI to distinguish the *ex vivo* tumor region from the surrounding healthy tissue has been explored. The samples were collected after the surgery and transported to the PA laboratory. Following the removal

of hairs from the samples, sutures were attached to hold the samples in a container filled with salt solution. The 3D scan of the sample with both ultrasound and PA images was acquired (see Fig. 3.3). The samples were sent for histopathological examination following the imaging. In the following sections, the literature review of various skin cancers imaged with PAI along with their use in this thesis is described.
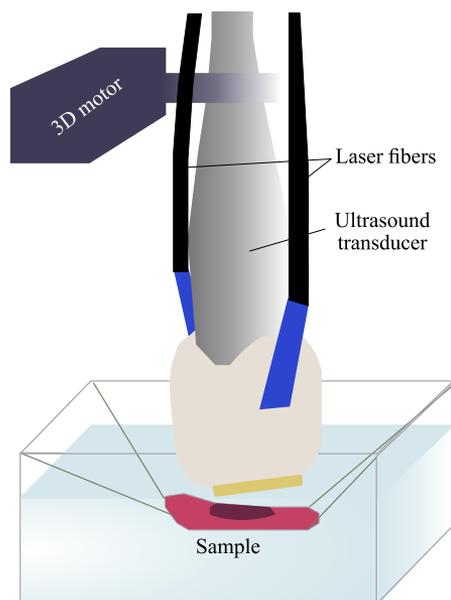
Figure 3.3: Illustration of the PAI system for *ex vivo* skin cancer imaging.

Malignant melanoma

MM cancers originate from melanocytes in the epidermis layer and are the deadliest kind of skin cancers [63]. PAI has demonstrated encouraging results in detecting MM borders and analyzing their molecular composition. The most dominant chromophore in the PA signal of these samples is melanin [61], [64]. In papers II and V, the feasibility of using two developed techniques to distinguish these tumors from the surrounding healthy tissue was investigated.

Basal cell carcinoma

BCCs are the most common skin tumors. In terms of chromophore contributions to the PA signal, there is a lower melanin contribution compared to the MM. Analysis

of eyelid BCCs samples showed higher HbO_2 contribution compared to the adjacent healthy tissues due to higher vascularization to transfer nutrition and oxygen to the tumors [62]. In paper V, the frequency analysis of PAI was utilized as a non-invasive tool to detect these tumors from the surrounding healthy tissue.

Cutaneous squamous cell carcinoma

CSCC cancer cells are the second most common type of non-melanoma, originating from the keratinocytes in the epidermis layer. High exposure to the UV light and aging are two risk factors for developing this kind of tumor [65]. PAI has shown great ability to visualize the tumor border in CSCCs samples in the wavelength range of 765 nm to 960 nm using tumors' unique spectral signatures [66].

Chapter 4

Tissue-mimicking phantoms

4.1 The role of phantoms

The demand for tissue-mimicking phantoms (TMPs) has grown with the advancement of novel multimodal imaging techniques such as PAI. These TMPs are essential for calibrating and routine control of imaging systems prior to the measurement, assessing the performance of novel quantitative methods, providing a standardized approach for comparative studies, and aiding in clinical training [40], [67]. TMPs used for PAI need to mimic both acoustic and optical tissue properties. The most critical properties include acoustic attenuation, speed of sound, optical scattering, and absorption [68]. TMPs should ideally be long-lasting, capable of being stored at room temperature, inexpensive, easy to produce, and tunable for desired properties [40], [69].

4.2 Fabrication and characteristics of phantoms

In this thesis, various types of phantoms suitable for PAI imaging have been developed and used, as described below. The use of these phantoms offers a ground truth, which is essential for the development of new methods.

4.2.1 Agar-based phantoms

Agar-based phantoms are straightforward to produce. They are created by mixing agar (Agar-Agar, Merck KGaA, Darmstadt, Germany) with water. The solution needs to be heated while stirring until the agar dissolves in the water. Next, the solution can be poured into a mold and allowed to cool at room temperature or in a refrigerator.

These phantoms exhibit a speed of sound close to soft tissues. Their acoustic attenuation properties can be adjusted by incorporating ingredients, such as graphite powder, which has been utilized to increase attenuation to the values compatible with soft tissue [70]. Agar-based phantoms usually mix with additives like titanium dioxide and inks to tune their optical properties similar to human tissue, such as skin layers [71]. In paper III, to enhance the PA signal, water-based colors were added to the agar phantom to make them suitable for PAI measurements (see Figure 4.1(a)). These TMPs are nontoxic, easy to fabricate, inexpensive, and have the flexibility of incorporating various additives. However, they are prone to bacterial degradation and have limited mechanical stability and long-term usage [72], [73].

4.2.2   SEBS phantoms

Oil-based materials are less prone to microbial degradation and dehydration, making them well-suited for producing tissue-mimicking materials (TMMs). In recent years, a gel made from copolymer styrene-ethylene/butylene-styrene (SEBS) in mineral oil has shown great potential due to its stable properties and optical and acoustic characteristics close to soft tissue [74], [75]. Additives can be used to tune their acoustic and optical properties. As an example, glycerol can be utilized to increase the speed of sound [75]. Pure SEBS gels show low optical absorption in the wavelength range suitable for PAI. To tune their optical properties, titanium dioxide, oil-soluble dyes, or commercial pigments can be utilized [76], [77]. In paper I, artists' oil-based inks in four colors dissolved and diluted in balsam turpentine are proposed to tune the optical properties of these phantoms. The optical and acoustic characteristics of TMMs with various colored inks and concentrations are investigated. The potential of oil-based SEBS phantoms with tunable optical characteristics in PAI is demonstrated by making heterogeneous smiley phantoms. These non-toxic TMPs are cost-effective, can be stored at room temperature, provide mechanical strength and long-term stability, and have the ability to tune their optical properties. However, fabrication of these phantoms requires heating the material to approximately 130 °C, making them unsuitable for incorporating additives that melt at such high temperatures, such as polyethylene microspheres. In addition to paper I, these phantoms have been used in paper II for making a TMP with various sizes of inclusions (see Figure 4.1(b)).

4.2.3   Microspheres phantoms

To test the effect of various sizes of particles in changing the content of the PA signal, phantoms containing polyethylene microspheres (Cospheric, Santa Barbara, CA, USA) can be produced [78]. These phantoms were prepared by adding mineral oil

into the colored microspheres of green and blue at a concentration of 1% by mass and pouring the solution into a cuvette as shown in Figure 4.1(c). The liquid forms of these phantoms were easy to prepare, but they showed issues such as aggregation and sticking to the inner walls of the cuvette, which required shaking before the PAI measurements. These phantoms were used in Paper IV. The solid form of these phantoms was created by incorporating microspheres into an agar solution to solve the aggregation problem.
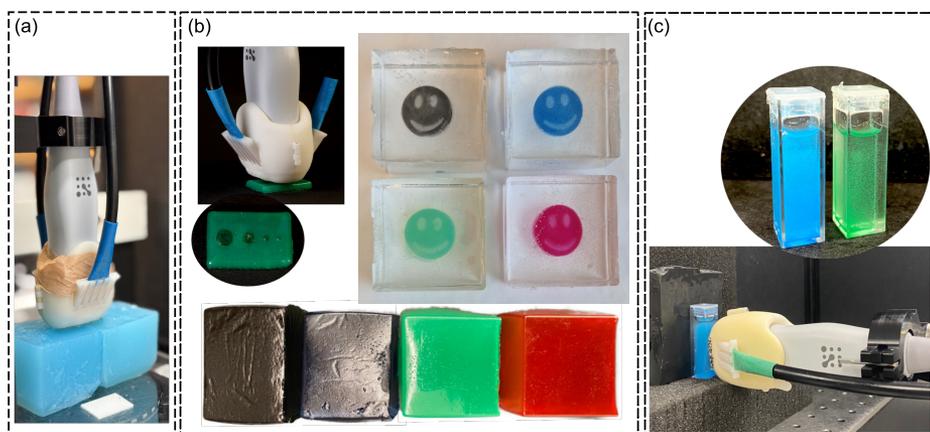
Figure 4.1: Various types of tissue-mimicking phantoms used in this work: (a) Agar-based phantoms, (b) SEBS-based phantoms, and (c) Microsphere-based phantoms.

Chapter 5

Processing approaches in photoacoustic imaging

5.1 Spectral unmixing

In multispectral PAI, the tissue is illuminated with multiple wavelengths, and multispectral images are acquired. The optical absorption of chromophores, and thus the PA response, varies with the wavelength of the transmitted laser pulse. This provides a specific spectral signature for each tissue chromophore [18], [66]. Spectral unmixing is a well-known technique that enables the classification of various optical absorbers based on their distinct spectral signatures. It has shown a high ability to classify the target of interest from the absorbing background using both exogenous contrast agents, such as Indocyanine green and metal nanoparticles [79], [80], and endogenous contrast agents, such as hemoglobin, melanin, fat, collagen, and water [81], [82]. Spectral unmixing has been employed in the detection of skin cancers [61], [62], blood oxygenation mapping [49], [53], [83], detection of instable carotid plaque [84], breast cancer diagnosis [85], and monitoring the cancer treatment [51].

Spectral unmixing techniques aim to decompose the PA spectra at each pixel into contribution maps of a set of chromophores based on their spectral signature [86]. The effectiveness of spectral unmixing methods relies on the range of excitation wavelengths, the spectral signature of tissue chromophores and tissue type, the number of chromophores involved, and the ability to distinguish the chromophore of interest from the background tissue [87]. Several spectral unmixing approaches have been developed, such as linear spectral unmixing, statistical sub-pixel detection, and blind source unmixing methods [88], [89].

5.1.1   Linear spectral unmixing

In the linear spectral unmixing, the measured PA spectrum in each pixel indicated as $P(r, \lambda)$, is modeled as a linear combination of the spectral signatures of a set of chromophores, $S_i(\lambda)$, with the weights indicating their fractional contribution to the measured spectra, $C_i(r)$[90], [91].

$$P(r, \lambda) = \sum_{i=1}^{K} C_i(r) S_i(\lambda) \tag{5.1}$$

where r denotes the spatial location, λ is the wavelength of the laser, and K represents the number of chromophores present in the tissue. This problem can be solved using non-negative least squares to estimate the fractional contributions, ensuring that the respective coefficients remain non-negative to be realistic [49]. The spectral signatures of chromophores can either be chosen from known spectra, such as those of hemoglobin, melanin, and water, or be estimated from tumor or healthy tissue. In paper III, linear spectral unmixing was applied to PA data with and without spectral coloring compensation to estimate oxygen saturation. Linear spectral unmixing is the most widely used unmixing method due to its simplicity [92]. However, it requires prior knowledge of all chromophores present in the tissue, and the lack of relevant chromophores can introduce errors in the estimated relative contribution maps [52]. Furthermore, it may be challenging to identify low-absorbing chromophores in the presence of dominant background absorption spectra [93]. In addition to the paper III, in paper I, linear spectral unmixing has been utilized to show the distribution map of oil-based inks in smiley phantoms. Figure 5.1 shows an example of linear spectral unmixing applied to the PA signals from finger data, segmented into three anatomical layers: epidermis, dermis, and hypodermis. The epidermis layer can be distinguished in the ultrasound image. However, the boundary between the dermis and hypodermis is not clearly visible, so an approximate dermis thickness of 1 mm was used to separate these two layers [56]. The average PA signal from these layers, the fitted spectrum, and the contribution map of each chromophore are shown. As shown, the signal in the epidermis layer is primarily dominated by melanin contributions from melanocytes. The dermis layer contains HbO_2 and HbR, reflecting the vascular plexus. In the hypodermis layer, the signal from blood and fat is dominant, consistent with the anatomical presence of subcutaneous fat in this layer that has been shown in a previous study by our group [49].

(a)

(b)
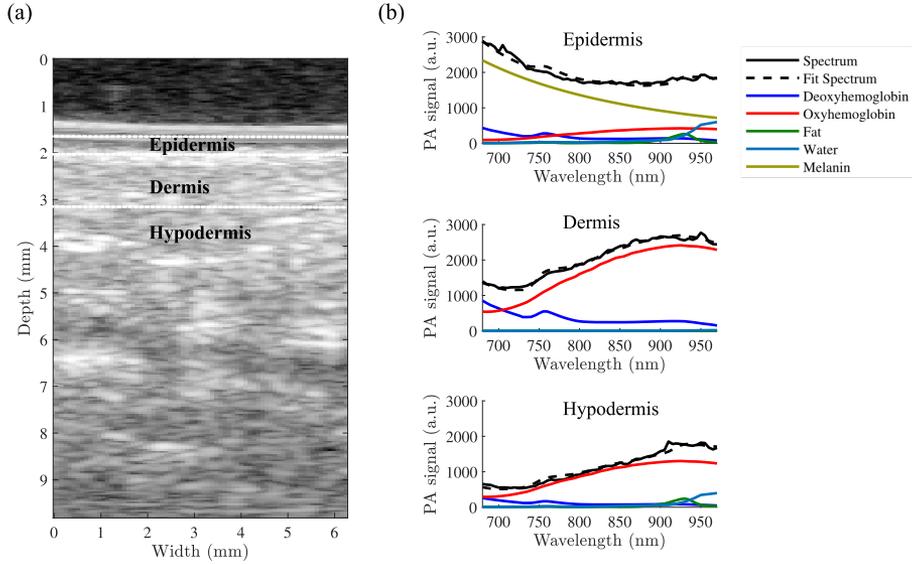
Figure 5.1: (a) Ultrasound image of finger where epidermis, dermis, and hypodermis are separated with a dashed line. (b) Linear spectral unmixing was applied to the averaged PA signal in each layer, where the received PA spectrum, fitted spectrum, and the contribution of each chromophore are shown.

5.1.2 Adaptive matched filter

Adaptive matched filter (AMF) is a statistical sub-pixel target detection approach [88]. A pixel-wise detection value D at each location in the image is estimated, which presents the similarity between the target and proposed pixel spectrum. AMF can be calculated using the formula below:

$$D(x_r) = \frac{(\mu_t - \mu_b)^{\mathrm{T}} \Sigma^{-1} (x_r - \mu_b)}{(\mu_t - \mu_b)^{\mathrm{T}} \Sigma^{-1} (\mu_t - \mu_b)}, \tag{5.2}$$

where μ_t is the target spectrum, μ_b is the background spectrum, Σ represents the background covariance matrix, T shows the matrix transpose operation, and x_r corresponds to the multispectral data at position r [94]. Applying a threshold to D divides pixels into either the target or the background. In the AMF models, the background spectral variability is modelled as a multivariate Gaussian distribution. AMF spectral unmixing technique can be used when the target spectrum is known, but there is no information on the specific background chromophores' spectra [87]. This assumption

makes this method suitable for skin cancer detection, where the target can be set to the skin tumor spectrum. It has also been shown that AMF methods can increase the detection sensitivity compared to the linear spectral unmixing and are more robust in the case of sparse targets present in the background [91], [93]. In paper II, AMF has been used as an unmixing method to delineate the MM tumors from the healthy tissues.

5.1.3   Blind source unmixing

In this unmixing approach, no prior knowledge of chromophores' absorption spectra is needed. Independent component analysis (ICA) and principal component analysis (PCA) have been used as two blind source approaches to find the exogenous contrast agents from the absorbing background [89]. Recently, Non-negative matrix factorization, which assumes non-negative sources, has shown great potential in separating the exogenous contract agents in PAI [80]. Although these approaches can be used to automatically separate the target of interest from the background, they may also generate components that represent no real chromophore spectrum, limiting their clinical interpretation [89], [95].

5.2   Spectral coloring compensation

Laser wavelength and tissue composition affect the propagation of light fluence through tissues, resulting in a spatially variant and wavelength-dependent absorption pattern. For instance, a uniform fluence spectrum at the surface of the tissue will be nonuniform when reaching deep tissue. This alternation to the light fluence leads to changes in both the amplitude and shape of the PA spectrum, called "spectral coloring" [93], [96], [97] (see Figure 5.2). In this figure, the changes to the PA spectra in a homogeneous blue phantom due to spectral coloring are shown. This corruption of PA spectra is an important and complex issue in the quantitative PAI. Uncertainty in light fluence as a function of depth contributes to errors in the interpretation of PA data, which subsequently affects the accurate quantification of tissue chromophore concentrations, particularly in deeper tissue [98].

Compensating for spectral coloring has been a key focus in quantitative PAI research. To compensate for the spectral coloring, light fluence distribution information in the tissue is needed. However, the complexity and computational time of these methods limit their clinical application. Several model-based techniques have been utilized, including Monte Carlo simulations [99]–[101] and approaches using the diffusion equation [102], [103]. However, these methods require prior knowledge of the tissue's optical properties. Another category of methods involves eigenspectra-based
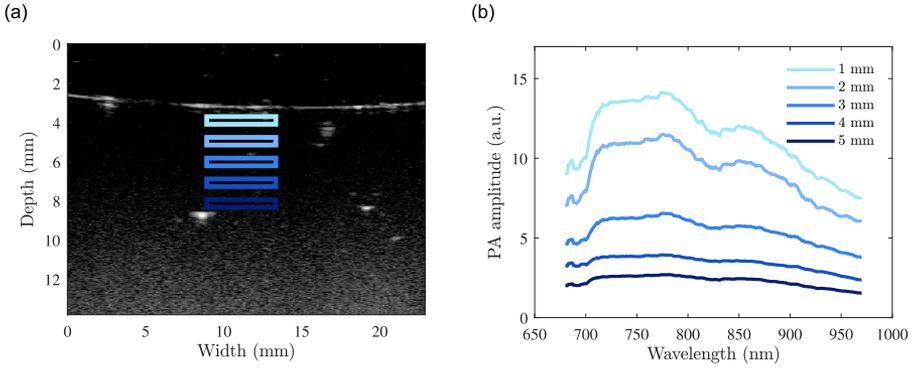
Figure 5.2: Spectral coloring effect in tissue-mimicking phantom. (a) Ultrasound image of a homogeneous phantom. (b) PA spectra at various depths of regions of interest (ROIs) from 1 mm to 5 mm below the surface show changes not only in amplitude but also in spectral shape.

approaches, which decompose the light fluence into a set of eigenspectra at each location in the image to estimate the tissue sO_2 [37]. Moreover, the use of frequency information of radio frequency (RF) PA data has been used to estimate the light fluence in the tissue [104]. Machine learning-based methods constitute another class of post-processing techniques that tend to compensate for the spectral coloring. As data-driven approaches, they require extensive training datasets and are highly dependent on the quality and realistic nature of these data for clinical applications [105]–[108]. In paper III, two spectral coloring approaches that exist in the literature were modified to be adopted to our *in vivo* human data and PAI system. Their performance was then evaluated and compared using the same finger dataset for estimating the oxygenation.

5.3 Frequency analysis

Despite progress in the quantitative PAI, the frequency analysis of RF PA data has gained less attention over the years. The frequency analysis of RF PA data usually involves extracting quantitative parameters from the linear model fitted to the normalized power spectra. The common parameters encompass midbandfit, intercept, and slope. Previous studies have shown the relation of these parameters with changes in concentration and size of optical absorbers [78], [109]. These parameters have been used as quantitative measurements to distinguish the cancer cells from the healthy tissue [110]–[113] and monitor the responders to thermosensitive liposome treatment

in breast cancer tissue [114].

Our group has utilized another quantitative parameter, center frequency (CF) of ultrasound RF data, for tissue characterization. The feasibility of using the CF in the ultrasound for tissue characterization has been demonstrated in plaque analysis, where high-risk carotid plaques have been identified by analyzing the CF of ultrasound data [115]. Furthermore, this parameter has been used in determining the arteries affected by giant cell arteries from the ones without [116]. In this thesis, the feasibility of using the CF spectrum in PA data for tissue characterization was investigated using both phantom and clinical data.

The CF is defined as the frequency at which most of the signal's energy is concentrated. The CF is calculated in the time domain using the autocorrelation function. This estimate has been used in Doppler ultrasound imaging for observing blood flow in real-time [117]. This calculation enhances accuracy and reduces noise, as well as overcomes the trade-off between time and frequency resolution compared to FFT analysis [118], [119]. Using an autocorrelation function, the phase difference between two consecutive samples can be calculated. The autocorrelation function, $R(n)$, is given by

$$R(n) = \frac{1}{N} \sum_{i=n-\frac{N}{2}}^{n+\frac{N}{2}} RF(i) \cdot RF^*(i-1) \tag{5.3}$$

where the beamformed RF data at sample i is represented by $RF(i)$ and $RF^*(i-1)$ shows the complex conjugate of data at sample $i-1$. N shows the size of averaging window and n is the sample in the axial direction.

This phase shift can be converted to actual frequency (CF) by

$$CF(n) = \frac{f_s}{2\pi} \arctan\left(\frac{Im(R(n))}{Re(R(n))}\right) \tag{5.4}$$

where f_s represents the sampling frequency, and Re and Im show the real and the imaginary content of the autocorrelation function [119].

The CF value can be estimated using Equation 5.4. By varying the wavelength of light, the corresponding CF values across the optical spectral range can be determined for each pixel, defined as CF spectrum. CF spectrum represents the mean frequency with respect to wavelength and conveys information about tissue properties. In Paper IV, the CF spectrum is defined for the first time, and its potential to distinguish phantoms of microspheres with varying sizes and colors is explored. In paper V, the CF spectrum analysis has been used to distinguish the *ex vivo* MM and BCC skin cancers from the healthy tissue. In addition, changes in the CF spectrum with vary-

ing oxygenation levels in the *in vivo* finger by using an occlusion-recovery model were also explored.

Chapter 6

Summary of papers

The five papers included in this thesis are all connected to the development of PAI and how to improve the clinical usage of this imaging modality. The connection of each paper's content to the thesis has been shown in the Figure. 6.1.
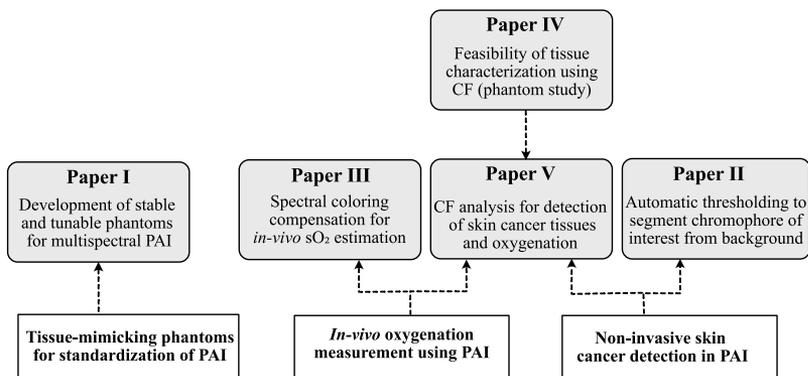
Figure 6.1: Block diagram illustrating the connection of each of the five parts of this thesis to the development and clinical translation of PAI.

As shown in Figure. 6.1, Paper I focuses on developing and characterizing tissue-mimicking phantoms for PAI. Paper III and part of paper V address *in-vivo* oxygenation measurements. Paper II and another part of paper V present non-invasive approaches for the detection of skin cancers. Paper IV explores the feasibility of using CF spectra for tissue characterization in a phantom study, the findings of which contributed to the further development of paper V.

6.1   Paper I: Optical Tuning of Copolymer-in-oil Tissue-mimicking Materials for Multispectral Photoacoustic Imaging

Tissue-mimicking materials (TMMs) are crucial for producing robust phantoms. These phantoms are essential for the calibration and evaluation of the performance of novel imaging systems, routine control of these systems, and assessment of new quantitative methods. In this paper, a gel consisting of SEBS in mineral oil was used as a base material. Furthermore, oil-based inks in four colors, carbon black, prussian blue, light green, and rubine magenta dissolved in turpentine, were added to tune the optical absorption properties of these phantoms. Various phantoms with different concentrations of SEBS-gel and oil-based inks were produced using cuvettes and cubic containers.

The optical properties of the phantoms, including the correlation between oil-based ink concentrations and their corresponding optical absorption, were investigated using collimated transmission spectroscopy in the wavelength range of 450–1550 nm. Subsequently, the speed of sound and acoustic attenuation coefficients were measured using the transmission method in a water tank filled with deionized water. Finally, multispectral PAI of the phantoms in a wavelength range of 680–970 nm was conducted.

The pure SEBS gel, without any additives or inks, exhibited translucency across the examined wavelength range. In contrast, the incorporation of oil-based inks dissolved in turpentine proved effective for accurately tuning the optical properties of the phantoms. Incorporating oil-based inks into the SEBS-gel showed no effect on changing the speed of sound of these phantoms. For two of the colors, rubine magenta and prussian blue, no clear relationship was observed between the acoustic attenuation coefficient and the mass fraction of oil-based inks. However, a slight decrease in acoustic attenuation was noted for the other two pigments, which may be attributed to a reduction in the SEBS mass fraction by adding larger volumes of oil-based inks.

Different colors of oil-based inks exhibited distinct PA spectra, while increasing their concentration resulted in higher PA amplitudes without altering the spectral shape. TMMs demonstrated long-term stability, while a repeated measurement after 14 months revealed the same PA spectra across different ink colors. Furthermore, a consecutive 12-minute measurement showed the highest temperature and PA amplitude increase in carbon black, which can be explained by the correlation between temperature and PA signal amplitude (see Fig. 6.2). Their applicability in supporting the clinical translation of PAI, including the investigation of spectral coloring effect, was also demonstrated. This was achieved by calculating the PA spectra in a homogeneous phantom as a function of depth from the surface. Furthermore, the feasibility

of producing custom-shaped phantoms was shown, while their 3D abundance maps were visualized using the linear spectral unmixing.
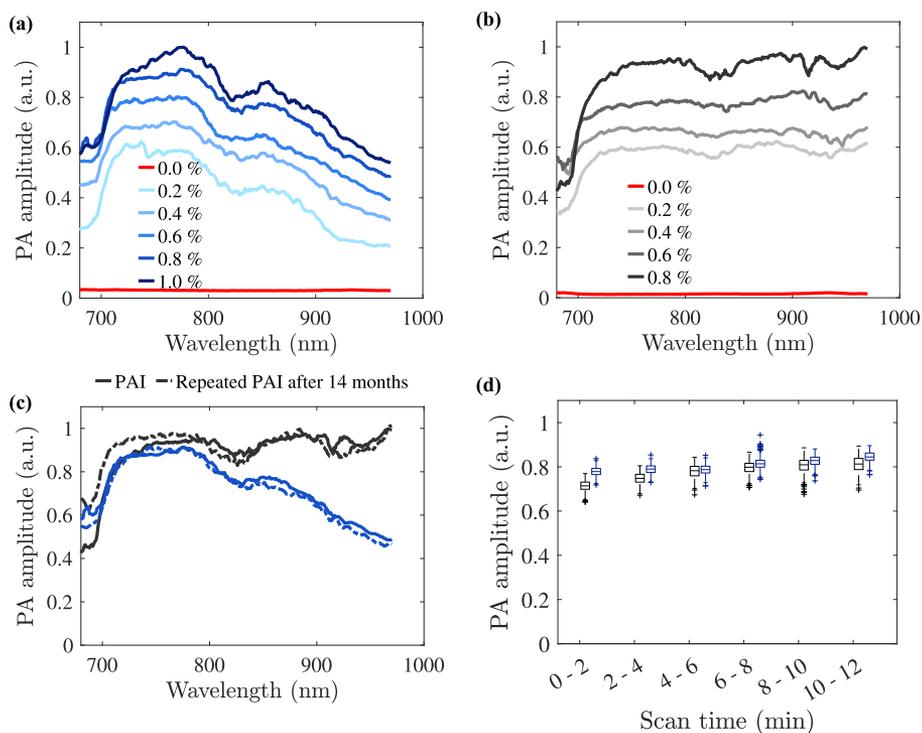

Figure 6.2: Example of PA spectra of two TMPs with varying concentrations of oil-based inks in (a) Prussian blue and (b) Carbon black. (c) Stability of PAI measurements for both TMPs at a concentration of 0.8 %, comparing the first measurement and a repeated one after 14 months. (d) Box plots showing the amplitude of the PA signal at a wavelength of 760 nm in a consecutive measurement.

6.2 Paper II: Automatic Threshold Selection Algorithm to Distinguish a Tissue Chromophore from the Background in Photoacoustic Imaging

The AMF is a statistical sub-pixel detection unmixing method for classifying the target (chromophore of interest) from absorbing background in PAI. Using the multispectral PA images and applying the AMF spectral unmixing results in a detection image in which the pixels' amplitude is proportional to the target probability. However, a threshold is required to be applied to the AMF detection image to separate the chromophore of interest from the background. This threshold is important since it allows us to estimate the thickness and width of the tumors, which are parameters related to the tumors' invasive stage. Selecting a threshold manually by highly skilled operators may introduce bias into the outcome. Therefore, automated approaches for threshold selection are necessary to improve reproducibility. In this paper, we have proposed an automatic threshold selection (ATS) algorithm that can be applied to the AMF detection image to classify the target from the absorbing background.

The method uses two features extracted from the AMF detection image: the number of connected components and the number of pixels in the largest connected component, to find the suitable threshold that separates the target from the background. To validate the approach, a SEBS tissue-mimicking phantom with four hemispherical inclusions was designed, and 3D multispectral PAI was performed. Furthermore, the method was applied to seven MM skin samples, and the thickness and width of the tumors, together with the delineation, were estimated and compared with histological examination.

The root mean squared error between the estimated thickness obtained using the ATS algorithm and the ground truth values was 0.26 mm for the phantom inclusions and 0.19 mm for the MM skin samples. The use of the ATS algorithm resulted in lower absolute errors in tumor thickness and width measurements compared to applying fixed threshold values to the AMF image (see Fig 6.3). In this study, the feasibility of using ATS in determining the thickness and width of MM skin samples without a highly skilled operator is demonstrated.
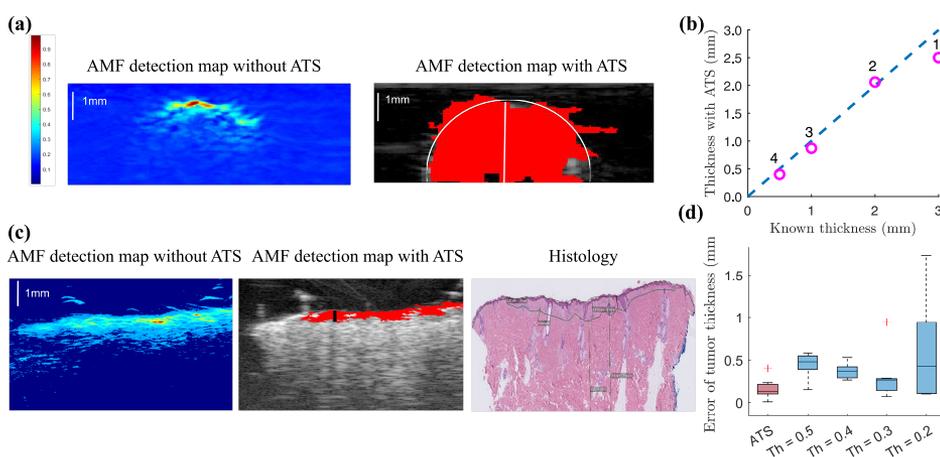
Figure 6.3: Example of result obtained for the largest inclusion in a TMP (a) AMF detection map without and with ATS, where the approximate extent of the inclusion and its thickness in shown. (b) Comparison of the thickness of four inclusions in a TMP with the known values. (c) An example of the AMF detection map in *ex vivo* human sample of MM without and with ATS, and the histological slide showing the thickness and extent of the tumor. (d) Boxplot of the absolute difference of the tumor thickness estimate with ATS and a number of fixed thresholds in MM tissue samples.

6.3   Paper III: Two Photoacoustic Spectral Coloring Compensation Techniques Adapted to the Context of Human In-vivo Oxygenation Measurements

Monitoring the sO_2 in the body provides valuable information about blood perfusion, health of the cardiovascular system, and the respiratory system. Furthermore, it has been shown to be a key biomarker in cancer treatment and monitoring. The spatial map of sO_2 in the body can be measured using the PAI and the endogenous chromophores in the body. However, the accuracy of *in-vivo* sO_2 estimation, especially in deeper tissue, is affected by the spectral coloring effect. A wavelength-dependent light attenuation that alters the PA spectra as light penetrates deeper into the tissue. Consequently, this results in uncertainty in the estimation of chromophore concentration.

In this paper, the performance of two previously proposed techniques to compensate for the spectral coloring was compared on the same *in vivo* human data. Both methods build upon existing approaches and are modified to be adapted to the context of human *in-vivo* and our PAI system. The first method uses the frequency content of RF PA data to estimate the fluence changes based on the slope of a linear fit to the ratio of power spectra at two wavelengths, called "method A". The second method utilizes eigenspectra decomposition to model the light fluence at each location in the image, called "method B". Both methods were modified, including automatic skin and epidermis segmentation to correct for the non-flat surface of the skin and the lack of hemoglobin in the epidermis layer, an automatic bandwidth selection accounting for lower frequency content of *in-vivo* data, adding more chromophores to improve accuracy, and usage of more wavelengths.

An agar-based tissue-mimicking phantom was used to evaluate the first method's performance, where an induced spectral coloring situation was created using a green agar phantom with three concentrations on top of a black agar phantom. Spatial map of sO_2 using the 10 human finger data with both methods was estimated. The performance of these methods was compared to the classic linear unmixing. The gradient of sO_2 with respect to depth has been used as a parameter to compare the performance of spectral coloring compensation techniques.

In the tissue-mimicking phantom, using method A, the original spectrum of the black phantom was restored by decreasing the relative mean square from 65% to 1.2% when using the highest concentration of green phantom. Both methods yielded similar sO_2 estimates and minimized the depth-dependent variations in sO_2 that are commonly observed with linear unmixing, reducing the gradient of saturation as a function of depth as physiologically expected in a normal situation (see Fig. 6.4).

(a)

(b)

(c)
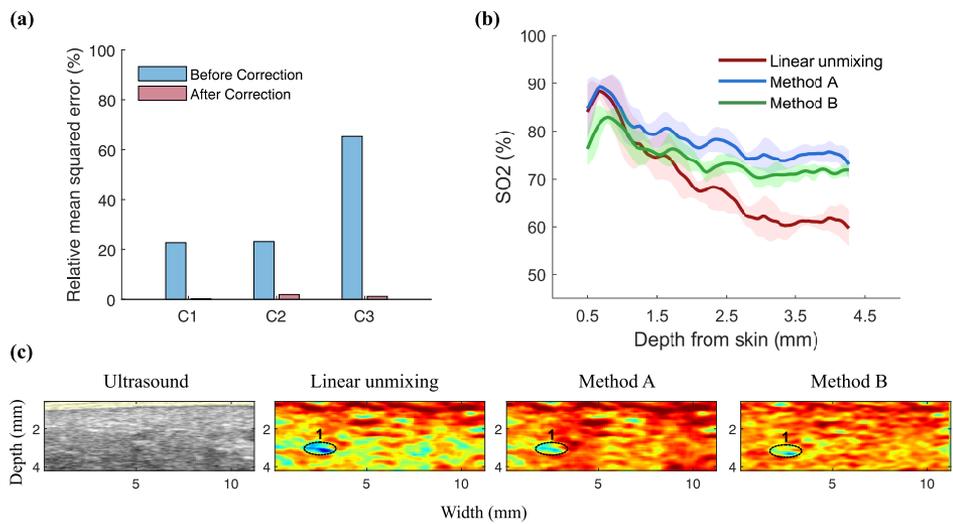
Figure 6.4: (a) The relative mean squared error (%) between the black phantom spectrum and the reference spectrum before and after correction using three different concentrations of the green phantom (0.25, 0.5, and 1 µl/ml). (b) The mean and standard deviation of sO_2 in one subject after 10 repetitive measurements. (c) Ultrasound image and spatial sO_2 maps in *in vivo* human finger of the same subject using Linear unmixing, method A, and method B. The observed sO_2 values for the selected roi (vein) are 44%, 59%, and 60%.

6.4 Paper IV: The Feasibility of Using Center Frequency Spectra in Photoacoustic Imaging for Tissue Characterization

The amplitude of the PA signal over the wavelength range, PA spectra, conveys information about the optical absorption of various chromophores in the body. Despite a great interest in the PAI analysts, fewer studies have explored the frequency content of PA data. In this study, we introduced the use of CF spectra as the mean frequency with respect to the wavelength. Here, in a phantom study, the effect of two parameters, color and size, on changing the CF spectra was explored.

Phantoms were manufactured by mixing mineral oil with microspheres of various sizes and two different colors: green and blue. The prepared mixtures were poured into cuvettes, and the PAI measurement of these phantoms using the MX400 ultrasound transducer was performed.

Microspheres with green and blue pigmentation in the same size exhibited different CF spectra shapes. The reason for the two distinct PA spectra could be that various colors absorb the laser energy differently over the wavelength range. Moreover, larger microspheres resulted in a lower CF offset. This could happen because larger microspheres develop a slower thermal expansion and generate lower frequency content (see Fig. 6.5). These findings suggest that CF analysis has the potential for distinguishing chromophores with varying optical properties within biological tissues.
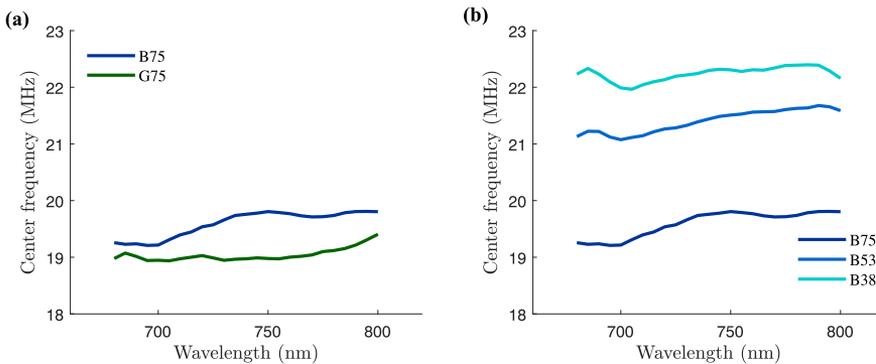
Figure 6.5: The CF spectra in TMPs with (a) Colors of blue and green and the same size of approximately 75 μm. (b) Color of blue and various sizes of approximate 75 μm, 53 μm, and 38 μm.

6.5 Paper V: Center Frequency Spectrum Analysis in Photoacoustic Imaging for Clinical Tissue Characterization

The frequency information of RF PA data is related to the absorbers' properties, such as size and shape. This study explores the possibility of using CF analysis in differentiating the *ex vivo* MM and BCC skin samples from the healthy tissue in a clinical setting. Furthermore, the changes in the CF spectra in an occlusion-recovery model using *in vivo* human finger data are investigated.

CF is estimated using phase differences between consecutive RF PA data. By calculating the CF for all wavelengths, a CF spectrum is acquired. CF contains information about the tissue properties and imaging system. A normalization was employed to remove the system dependency, and the normalized CF spectrum was defined as the alpha spectrum. The shape and the slope of the linear model fitted to the alpha spectra were investigated as potential biomarkers to differentiate between the tumors and healthy tissue, and the changes in the oxygenation.

Analysis of the normalized alpha spectra revealed statistically significant differences at 42 and 29 out of 59 wavelengths for MM and BCC tumors, respectively, when compared to healthy tissue. Furthermore, the median of alpha spectral slopes demonstrated significant differences with p-values of less than 0.05 and 0.001 for MM and BCC tumor parts and healthy tissue, respectively, with higher alpha slope values observed in the tumor regions (see Fig. 6.6). In the occlusion-recovery measurement, the normalized alpha spectra revealed statistically significant differences at 36 out of 59 wavelengths with a 60% decrease in the normalized alpha value at 755 nm during the occlusion phase. The median of the alpha spectral slope in all subjects revealed a statistically significant difference (p-value< 0.05) between the occlusion and recovery phases, with a higher slope for the occlusion phase.

In this study, the CF is calculated in the time domain, which overcomes the trade-off between time and frequency resolution. The slope of a linear model fitted to the alpha spectra indicated the ability of this spectral parameter as a potential biomarker, with tumors exhibiting consistently higher slope values compared to healthy tissue. Furthermore, a higher alpha slope was observed in the occlusion phase compared to the recovery phase. These findings indicate that CF spectrum analysis could serve as a potential biomarker for non-invasive skin tumor detection. It is also capable of tracking oxygenation changes in tissue.
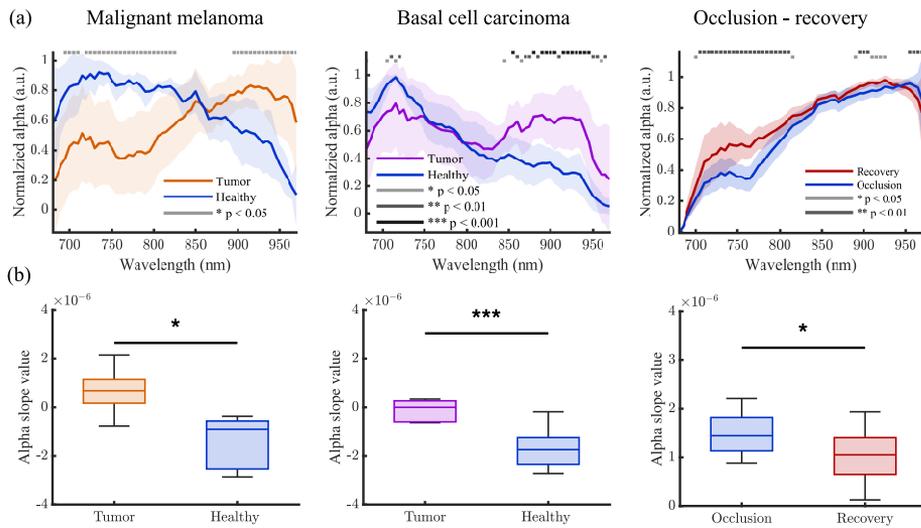
Figure 6.6: (a) Normalized alpha spectra with dashed lines indicating different levels of significance in MM, BCC, and oxygenation measurements. (b)The median alpha spectral slopes show significant differences between MM and BCC tumors and healthy regions, as well as between the occlusion and recovery phases.

Chapter 7
Conclusion and outlook

7.1 Conclusion

PAI is an innovative imaging technique with a wide range of potential clinical applications. This thesis mainly focused on technical developments to facilitate PAI clinical usage in the future, addressing the aims outlined in chapter 1. All papers in this thesis are connected by three central themes in PAI: the development of TMPs for performance evaluation, non-invasive skin cancer detection, and *in vivo* oxygenation measurements. In this chapter, the key conclusions from the projects, along with my reflections and suggestions for future work, are presented.

SEBS-gel, a non-toxic material which can be stored at room temperature, has been recently used to produce TMPs [69], [75]. Pure SEBS-gel has low intrinsic optical absorption, requiring the addition of pigments to tune its absorption properties [77]. However, there was a gap in the literature regarding the concentration-dependent effects of oil-based pigments on the PA spectra, as well as their depth-dependent behavior. Understanding these effects is crucial for the further development and validation of phantoms. In Paper I, we addressed this gap by developing a novel approach for creating TMPs using SEBS-gel, turpentine, and oil-based inks with tunable optical properties. These phantoms demonstrated long-term stability at room temperature and produced high PA signal amplitudes with different spectral shapes using various ink colors. Furthermore, we investigated the PA spectrum as a function of increasing the absorption and depth. I believe this optical tuning is an important step toward achieving the desired PA spectrum and more realistic phantoms. I also think that the development of such phantoms offers a robust platform for assessing and validating new technical methods in PAI.

PAI has shown potential to detect skin tumors non-invasively [64], [120], [121]. In my research group, non-invasive skin tumor detection has been a key objective, given access to human skin samples. However, most existing methods for skin tu-

mor detection rely on operator expertise. Our goal was to develop a more automatic approach to distinguish skin tumors from healthy tissue. In paper II, an ATS algorithm applied to AMF spectral unmixing showed better performance in estimating the thickness and width of MM tumors compared to using fixed threshold values. In this study, we demonstrated the potential of an automatic approach for tumor delineation in MM skin cancer. Additionally, since the PA amplitude spectra of BCC are difficult to distinguish from healthy tissue, there is a limitation in detection methods that only utilize the amplitude information. To address this, we explored the use of frequency-domain features, specifically the center frequency spectrum, as an alternative approach. In paper V, CF spectrum analysis using novel alpha spectral parameters demonstrated the ability to distinguish MM and BCC from healthy tissue. The alpha slope showed higher values in tumor regions, indicating its potential as a non-invasive biomarker for skin cancer detection. In this study, the use of frequency information of RF PA data was explored to address this challenge, and the results suggest a promising direction for future research. I believe these findings highlight PAI's promise for non-invasive skin cancer diagnostics.

PAI has the potential to estimate the spatial map of sO_2 in the body [53], [107]. In Paper III and a part of paper V, methods were used to explore the *in vivo* oxygenation. One of the aims of my project was to explore the common problem of spectral coloring in the context of human *in vivo* oxygenation. Paper III explores the adaptation of two spectral coloring approaches to our PAI system and *in vivo* oxygenation situations. Both methods effectively decreased the depth-dependent changes in sO_2, typically observed with linear unmixing. In paper V, for the first time, we investigated the potential of CF spectrum analysis in detecting the changes in the oxygenation. The alpha spectrum exhibited a shift toward higher slope values during the occlusion phase compared to recovery, indicating its potential for distinguishing between these physiological states. I think the observed change in the CF spectrum shape with varying oxygenation is a unique observation and has the potential to provide valuable insights. Paper IV introduces the CF spectrum in a TMP study, showing different CF spectra in phantoms with different colors and sizes. The findings of this paper served as a foundational step for further development of paper V.

Overall, the five papers included in this thesis aim to contribute to the development of PAI and to advance its potential for clinical applications.

7.2 Future works

The present thesis explores the potential clinical applications of PAI. In this thesis, I had the opportunity to work with human clinical data. However, future studies with larger clinical datasets will be beneficial in evaluating the methods' robustness.

In Paper I, the use of four different oil-based color inks resulted in distinct PA spectra. By combining various inks, it may be possible to produce spectra that more closely mimic the absorption characteristics of endogenous chromophores such as hemoglobin. This will be beneficial for testing new algorithms intended for clinical use, such as oxygenation estimation.

Furthermore, spectral coloring compensation approaches hold potential for applications in clinical contexts beyond sO_2 estimation and improving the accuracy of spectral unmixing in other clinical applications. For example, when it comes to deeper skin cancer tissues, spectral coloring compensation can improve tumor delineation, particularly for tumors with greater thickness.

In the context of skin cancer detection, comparative investigations across a broader range of skin cancers, including squamous cell carcinomas, could yield valuable insights. In papers IV and V, we introduced and utilized CF spectrum analysis for tissue characterization. While the slope of alpha spectra showed a significant difference between the tumors and healthy tissues, other spectral parameters within the alpha spectrum may also offer valuable diagnostic information. Furthermore, the observed changes in the shape of the alpha spectra during the occlusion and recovery phases open up interesting directions for future research, which could be linked to the endothelial function evaluation. In my opinion, the novel relationship between CF spectral features and varying tissue oxygenation levels is particularly promising and worth further investigation. In addition, spectral coloring may have less impact on frequency information such as CF, which remains a challenge when analysing *in vivo* clinical data. Finally, the combination of CF and PA spectra has the potential to enhance diagnostic accuracy, as the two approaches may provide complementary information.

In conclusion, the projects presented in this thesis contribute to the validation of methods' performances, advancement of non-invasive detection and delineation of skin cancers and *in vivo* oxygenation measurement. I believe that PAI holds strong potential for integration into clinical practice, either as a complementary tool to ultrasound or as an independent diagnostic modality.

References

[1]   P. Beard, "Biomedical photoacoustic imaging", *Interface Focus*, vol. 1, no. 4, pp. 602–631, 2011. doi: 10.1098/rsfs.2011.0028.

[2]   J. Weber, P. C. Beard, and S. E. Bohndiek, "Contrast agents for molecular photoacoustic imaging", *Nature methods*, vol. 13, no. 8, pp. 639–650, 2016. doi: 10.1038/NMETH.3929.

[3]   D. Das, A. Sharma, P. Rajendran, and M. Pramanik, "Another decade of photoacoustic imaging", *Physics in Medicine & Biology*, vol. 66, no. 5, 05TR01, 2021. doi: 10.1088/1361-6560/abd669.

[4]   A. B. E. Attia, G. Balasundaram, M. Moothanchery, *et al.*, "A review of clinical photoacoustic imaging: Current and future trends", *Photoacoustics*, vol. 16, p. 100 144, 2019. doi: https://doi.org/10.1016/j.pacs.2019.100144.

[5]   J. Park, S. Choi, F. Knieling, *et al.*, "Clinical translation of photoacoustic imaging", *Nature Reviews Bioengineering*, vol. 3, pp. 193–212, 2025. doi: https://doi.org/10.1038/s44222-024-00240-y.

[6]   A. G. Bell, "The photophone", *Science*, no. 11, pp. 130–134, 1880. doi: 10.1126/science.os-1.11.130.

[7]   A. G. Bell, "The production of sound by radiant energy", *Science*, no. 48, pp. 242–253, 1881. doi: 10.1126/science.os-2.48.242.

[8]   M. Vengerov, "An optical-acoustic method of gas analysis", *Nature*, vol. 158, no. 4001, pp. 28–29, 1946. doi: https://doi.org/10.1038/158028c0.

[9]   A. Rosencwaig and P. R. Griffiths, *Photoacoustics and photoacoustic spectroscopy*, 1981. doi: https://doi.org/10.1063/1.2914619.

[10]   R. O. Esenaliev, A. A. Karabutov, F. K. Tittel, *et al.*, "Laser optoacoustic imaging for breast cancer diagnostics: Limit of detection and comparison with x-ray and ultrasound imaging", in *Optical Tomography and Spectroscopy of Tissue: Theory, Instrumentation, Model, and Human Studies II*, SPIE, vol. 2979, 1997, pp. 71–82. doi: https://doi.org/10.1117/12.280213.

[11]   B. Cox, J. G. Laufer, S. R. Arridge, and P. C. Beard, "Quantitative spectroscopic photoacoustic imaging: A review", *Journal of Biomedical Optics*, vol. 17, no. 6, p. 061 202, 2012. doi: https://doi.org/10.1117/1.JBO.17.6.061202.

[12]   S. Y. Emelianov, P.-C. Li, and M. O'Donnell, "Photoacoustics for molecular imaging and therapy", *Physics Today*, vol. 62, no. 8, pp. 34–39, 2009. doi: https://doi.org/10.1063/1.3141939.

[13]   X. Wang, Y. Pang, G. Ku, X. Xie, G. Stoica, and L. V. Wang, "Noninvasive laser-induced photoacoustic tomography for structural and functional in vivo imaging of the brain", *Nature Biotechnology*, vol. 21, no. 7, pp. 803–806, 2003. doi: 10.1038/nbt839.

[14]   D. Jung, S. Park, C. Lee, and H. Kim, "Recent progress on near-infrared photoacoustic imaging: Imaging modality and organic semiconducting agents", *Polymers*, vol. 11, no. 10, p. 1693, 2019. doi: https://doi.org/10.3390/polym11101693.

[15]   L. V. Wang, "Tutorial on photoacoustic microscopy and computed tomography", *IEEE Journal of Selected Topics in Quantum Electronics*, vol. 14, no. 1, pp. 171–179, 2008. doi: 10.1109/JSTQE.2007.913398.

[16]   V. Ntziachristos, J. Ripoll, L. V. Wang, and R. Weissleder, "Looking and listening to light: The evolution of whole-body photonic imaging", *Nature biotechnology*, vol. 23, no. 3, pp. 313–320, 2005. doi: 10.1038/nbt1074.

[17]   S. Han, D. Lee, S. Kim, H.-H. Kim, S. Jeong, and J. Kim, "Contrast agents for photoacoustic imaging: A review focusing on the wavelength range", *Biosensors*, vol. 12, no. 8, p. 594, 2022. doi: https://doi.org/10.3390/bios12080594.

[18]   S. L. Jacques, "Optical properties of biological tissues: A review", *Physics in Medicine & Biology*, vol. 58, no. 11, R37, 2013. doi: 10.1088/0031-9155/58/11/R37.

[19]   A. Das, A. Ghosh, S. Chattopadhyaya, and C.-F. Ding, "A review on critical challenges in additive manufacturing via laser-induced forward transfer", *Optics & Laser Technology*, vol. 168, p. 109 893, 2024. doi: https://doi.org/10.1016/j.optlastec.2023.109893.

[20] B. T. Cox, S. R. Arridge, and P. C. Beard, "Estimating chromophore distributions from multiwavelength photoacoustic images", *JOSA A*, vol. 26, no. 2, pp. 443–455, 2009. doi: https://doi.org/10.1364/JOSAA.26.000443.

[21] T. Hawez, M. Evertsson, T. Erlöv, *et al.*, "The use of ultra-high frequency ultrasound in identifying aganglionosis in hirschsprung's disease", *Scientific Reports*, vol. 15, no. 1, p. 15 124, 2025. doi: https://doi.org/10.1038/s41598-025-99897-7.

[22] R. Sheikh, M. Cinthio, U. Dahlstrand, *et al.*, "Clinical translation of a novel photoacoustic imaging system for examining the temporal artery", *IEEE Transactions on Ultrasonics, Ferroelectrics, and Frequency Control*, vol. 66, no. 3, pp. 472–480, 2018. doi: 10.1109/TUFFC.2018.2868674.

[23] F. Cao, Z. Qiu, H. Li, and P. Lai, "Photoacoustic imaging in oxygen detection", *Appl. Sci.*, vol. 7, no. 12, p. 1262, 2017. doi: 10.3390/app7121262.

[24] M. A. Haidekker, *Medical imaging technology*, 2013.

[25] A. A. Stratonnikov and V. B. Loschenov, "Evaluation of blood oxygen saturation in vivo from diffuse reflectance spectra", *Journal of biomedical optics*, vol. 6, no. 4, pp. 457–467, 2001. doi: https://doi.org/10.1117/1.1411979.

[26] A. Villringer, J. Planck, C. Hock, L. Schleinkofer, and U. Dirnagl, "Near infrared spectroscopy (nirs): A new tool to study hemodynamic changes during activation of brain function in human adults", *Neuroscience letters*, vol. 154, no. 1-2, pp. 101–104, 1993. doi: https://doi.org/10.1016/0304-3940(93)90181-J.

[27] X. Hui, M. O. Malik, and M. Pramanik, "Looking deep inside tissue with photoacoustic molecular probes: A review", *Journal of biomedical optics*, vol. 27, no. 7, pp. 070 901–070 901, 2022. doi: 10.1117/1.JBO.27.7.070901.

[28] M. T. Rietberg, J. Gröhl, T. R. Else, S. E. Bohndiek, S. Manohar, and B. T. Cox, "Artifacts in photoacoustic imaging: Origins and mitigations", *arXiv preprint arXiv:2504.12772*, 2025. doi: https://doi.org/10.48550/arXiv.2504.12772.

[29] J. Shah, S. Park, S. Aglyamov, *et al.*, "Photoacoustic imaging and temperature measurement for photothermal cancer therapy", *Journal of biomedical optics*, vol. 13, no. 3, pp. 034 024–034 024, 2008. doi: https://doi.org/10.1117/1.2940362.

[30]   M. Bakaric, A. Ivory, B. Zeqiri, B. T. Cox, and B. E. Treeby, "Measurement of the temperature-dependent speed of sound and change in grüneisen parameter of tissue-mimicking materials", in *2019 IEEE International Ultrasonics Symposium (IUS)*, IEEE, 2019, pp. 1–4. doi: 10.1109/ULTSYM.2019.8925838.

[31]   M. E. Noltes, M. Bader, M. J. Metman, *et al.*, "Towards in vivo characterization of thyroid nodules suspicious for malignancy using multispectral optoacoustic tomography", *European Journal of Nuclear Medicine and Molecular Imaging*, vol. 50, no. 9, pp. 2736–2750, 2023. doi: 10.1007/s00259-023-06189-1.

[32]   B. E. Treeby, "Acoustic attenuation compensation in photoacoustic tomography using time-variant filtering", *Journal of biomedical optics*, vol. 18, no. 3, pp. 036008–036008, 2013. doi: https://doi.org/10.1117/1.JBO.18.3.036008.

[33]   S. Medical, *Seno med. Instrum. Receiv. CE Mark*, https://senomedical.com/newsroom/press-releases/newsroom-press-releases-2014-seno-medical-instruments-receives-ce-mark-for-imagio-breast-imaging-system, 2014.

[34]   iThera Medical, *CE mark awarded to iThera Medical*, https://ithera-medical.com/ce-mark-awarded-to-ithera-medicals-msot-acuity-optoacoustic-imaging-system/, 2021.

[35]   J. J. Riksen, A. V. Nikolaev, and G. van Soest, "Photoacoustic imaging on its way toward clinical utility: A tutorial review focusing on practical application in medicine", *Journal of Biomedical Optics*, vol. 28, no. 12, pp. 121205–121205, 2023. doi: https://doi.org/10.1117/1.JBO.28.12.121205.

[36]   S. Chandramoorthi, J. J. Riksen, A. V. Nikolaev, A. F. Van Der Steen, and G. Van Soest, "Wideband photoacoustic imaging in vivo with complementary frequency conventional ultrasound transducers", *Frontiers in Physics*, vol. 10, p. 954537, 2022. doi: https://doi.org/10.3389/fphy.2022.954537.

[37]   S. Tzoumas, A. Nunes, I. Olefir, *et al.*, "Eigenspectra optoacoustic tomography achieves quantitative blood oxygenation imaging deep in tissues", *Nat. Commun.*, vol. 7, no. 1, p. 12121, 2016. doi: 10.1038/ncomms12121.

[38]   G.-S. Jeng, M.-L. Li, M. Kim, *et al.*, "Real-time interleaved spectroscopic photoacoustic and ultrasound (paus) scanning with simultaneous fluence compensation and motion correction", *Nature communications*, vol. 12, no. 1, p. 716, 2021. doi: 10.1038/s41467-021-20947-5.

[39] G. S. Fernandes, J. H. Uliana, L. Bachmann, A. A. Carneiro, M. A. L. Bell, and T. Z. Pavan, "Mitigating skin tone bias in linear array in vivo photoacoustic imaging with short-lag spatial coherence beamforming", *Photoacoustics*, vol. 33, p. 100 555, 2023. doi: https://doi.org/10.1016/j.pacs.2023.100555.

[40] L. Hacker, H. Wabnitz, A. Pifferi, T. J. Pfefer, B. W. Pogue, and S. E. Bohndiek, "Criteria for the design of tissue-mimicking phantoms for the standardization of biophotonic instrumentation", *Nature Biomedical Engineering*, vol. 6, no. 5, pp. 541–558, 2022. doi: 10.1038/s41551-022-00890-6.

[41] C. Hartog and F. Bloos, "Venous oxygen saturation", *Best Pract. Res. Clin. Anaesthesiol.*, vol. 28, no. 4, pp. 419–428, 2014. doi: /10.1016/j.bpa.2014.09.006.

[42] D. R. McIlroy, M. S. Shotwell, M. G. Lopez, *et al.*, "Oxygen administration during surgery and postoperative organ injury: Observational cohort study", *Bmj*, vol. 379, 2022. doi: https://doi.org/10.1136/bmj-2022-070941.

[43] P. Schumacker and S. Cain, "The concept of a critical oxygen delivery", *Intensive care medicine*, vol. 13, no. 4, pp. 223–229, 1987. doi: 10.1007/BF00 265110.

[44] M. Gerling, Y. Zhao, S. Nania, *et al.*, "Real-time assessment of tissue hypoxia in vivo with combined photoacoustics and high-frequency ultrasound", *Theranostics*, vol. 4, no. 6, p. 604, 2014. doi: 10.7150/thno.7996.

[45] M. W. Wukitsch, M. T. Petterson, D. R. Tobler, and J. A. Pologe, "Pulse oximetry: Analysis of theory, technology, and practice", *J. Clin. Monit.*, vol. 4, pp. 290–301, 1988. doi: 10.1007/bf01617328.

[46] H. Jamali, L. T. Castillo, C. C. Morgan, *et al.*, "Racial disparity in oxygen saturation measurements by pulse oximetry: Evidence and implications", *Ann Am Thorac Soc*, vol. 19, no. 12, pp. 1951–1964, 2022, ISSN: 2329-6933. doi: 1 0.1513/AnnalsATS.202203-270CME. (visited on 03/22/2023).

[47] P. Kyriacou, K. Budidha, and T. Y. Abay, "Optical techniques for blood and tissue oxygenation", *Encyclopedia of Biomedical Engineering*, vol. 3, pp. 461–472, 2019. doi: 10.1016/B978-0-12-801238-3.10886-4.

[48] T. Strömberg, H. Karlsson, I. Fredriksson, F. H. Nyström, and M. Larsson, "Microcirculation assessment using an individualized model for diffuse reflectance spectroscopy and conventional laser doppler flowmetry", *Journal of Biomedical Optics*, vol. 19, no. 5, pp. 057 002–057 002, 2014. doi: 10.1117/1.JBO.19.5.057002.

[49] A. Merdasa, J. Bunke, M. Naumovska, *et al.*, "Photoacoustic imaging of the spatial distribution of oxygen saturation in an ischemia-reperfusion model in humans", *Biomed. Opt. Express*, vol. 12, no. 4, pp. 2484–2495, 2021. doi: 10. 1364/boe.418397.

[50] S. Gargiulo, S. Albanese, and M. Mancini, "State-of-the-art preclinical photoacoustic imaging in oncology: Recent advances in cancer theranostics", *Contrast media & molecular imaging*, vol. 2019, no. 1, p. 5 080 267, 2019. doi: h ttps://doi.org/10.1155/2019/5080267.

[51] M. N. Fadhel, S. Appak Baskoy, Y. Wang, E. Hysi, and M. C. Kolios, "Use of photoacoustic imaging for monitoring vascular disrupting cancer treatments", *J. Biophotonics*, vol. 16, no. 4, e202000209, 2020. doi: 10.1002/jbio.20200 0209.

[52] A. Merdasa, J. Berggren, K. Tenland, *et al.*, "Oxygen saturation mapping during reconstructive surgery of human forehead flaps with hyperspectral imaging and spectral unmixing", *Microvasc. Res.*, vol. 150, p. 104 573, 2023. doi: 10.1016/j.mvr.2023.104573.

[53] J. Bunke, A. Merdasa, R. Sheikh, *et al.*, "Photoacoustic imaging for the monitoring of local changes in oxygen saturation following an adrenaline injection in human forearm skin", *Biomed. Opt. Express*, vol. 12, no. 7, pp. 4084–4096, 2021. doi: 10.1364/boe.423876.

[54] Y. Gilaberte, L. Prieto-Torres, I. Pastushenko, and Á. Juarranz, "Anatomy and function of the skin", in *Nanoscience in dermatology*, Elsevier, 2016, pp. 1–14. doi: 10.1016/B978-0-12-802926-8.00001-X.

[55] J. T. Whitton and J. Everall, "The thickness of the epidermis", *Br. J. Dermatol.*, vol. 89, no. 5, pp. 467–476, 1973. doi: 10.1111/j.1365-2133.1973.tb03007. x.

[56] K. Mizukoshi, H. Iwazaki, and T. Ida, "Quantitative analysis of age-related changes in vascular structure, oxygen saturation, and epidermal melanin structure using photoacoustic methods", *Skin Research and Technology*, vol. 30, no. 1, e13537, 2024. doi: 10.1111/srt.13537.

[57] P. G. Agache, P. Humbert, and H. I. Maibach, *Measuring the Skin: Non-invasive Investigations, Physiology, Normal Constants*. Springer, 2004. doi: 10. 1007/978-3-319-32383-1.

[58] J. Reichrath, U. Leiter, T. Eigentler, and C. Garbe, "Epidemiology of skin cancer", *Sunlight, vitamin D and skin cancer*, pp. 120–140, 2014. doi: 10. 1007/978-1-4939-0437-2_7.

[59] D. Roberts, A. Anstey, R. Barlow, *et al.*, "UK guidelines for the management of cutaneous melanoma", *British Journal of Dermatology*, vol. 146, no. 1, pp. 7–17, 2002. doi: 10.1046/j.1365-2133.2001.04614.x.

[60] L. Cumberland, A. Dana, and N. Liegeois, "Mohs micrographic surgery for the management of nonmelanoma skin cancers", *Facial plastic surgery clinics of North America*, vol. 17, no. 3, pp. 325–335, 2009. doi: 10.1016/j.fsc.2009. 06.001.

[61] J. Hult, A. Merdasa, A. Pekar-Lukacs, *et al.*, "Comparison of photoacoustic imaging and histopathological examination in determining the dimensions of 52 human melanomas and nevi ex vivo", *Biomed. Opt. Express*, vol. 12, no. 7, pp. 4097–4114, 2021. doi: 10.1364/BOE.425524.

[62] M. T. Stridh, J. Hult, A. Merdasa, *et al.*, "Photoacoustic imaging of periorbital skin cancer ex vivo: Unique spectral signatures of malignant melanoma, basal, and squamous cell carcinoma", *Biomed. Opt. Express*, vol. 13, no. 1, pp. 410–425, 2021. doi: 10.1364/BOE.443699.

[63] D. Schadendorf, A. C. Van Akkooi, C. Berking, *et al.*, "Melanoma", *The Lancet*, vol. 392, no. 10151, pp. 971–984, 2018. doi: 10.1016/S0140-6736(18)31559-9.

[64] J. W. Fakhoury, J. B. Lara, R. Manwar, *et al.*, "Photoacoustic imaging for cutaneous melanoma assessment: A comprehensive review", *Journal of Biomedical Optics*, vol. 29, no. S1, S11518–S11518, 2024. doi: 10.1117/1.JBO.29.S1. S11518.

[65] M. C. Winge, L. N. Kellman, K. Guo, *et al.*, "Advances in cutaneous squamous cell carcinoma", *Nature Reviews Cancer*, vol. 23, no. 7, pp. 430–449, 2023. doi: 10.1038/s41568-023-00583-5.

[66] J. Hult, U. Dahlstrand, A. Merdasa, *et al.*, "Unique spectral signature of human cutaneous squamous cell carcinoma by photoacoustic imaging", *Journal of Biophotonics*, vol. 13, no. 5, e201960212, 2020. doi: 10.1002/jbio. 201960212.

[67] B. W. Pogue and M. S. Patterson, "Review of tissue simulating phantoms for optical spectroscopy, imaging and dosimetry", *Journal of biomedical optics*, vol. 11, no. 4, pp. 041 102–041 102, 2006. doi: 10.1117/1.2335429.

[68] W. C. Vogt, C. Jia, K. A. Wear, B. S. Garra, and T. Joshua Pfefer, "Biologically relevant photoacoustic imaging phantoms with tunable optical and acoustic properties", *Journal of biomedical optics*, vol. 21, no. 10, pp. 101 405–101 405, 2016. doi: 10.1117/1.JBO.21.10.101405.

[69] L. Hacker, J. Joseph, A. M. Ivory, *et al.*, "A copolymer-in-oil tissue-mimicking material with tuneable acoustic and optical characteristics for photoacoustic imaging phantoms", *IEEE Transactions on Medical Imaging*, vol. 40, no. 12, pp. 3593–3603, 2021. doi: 10.1109/TMI.2021.3090857.

[70] D. Oliveira, J. C. Júnior, R. Jaime, *et al.*, "Acoustic and thermal properties in agarose-based phantom with different graphite powder concentration", *city*, vol. 1000, p. 1, 2014.

[71] A. I. Chen, M. L. Balter, M. I. Chen, *et al.*, "Multilayered tissue mimicking skin and vessel phantoms with tunable mechanical, optical, and acoustic properties", *Medical physics*, vol. 43, no. 6Part1, pp. 3117–3131, 2016. doi: 10.1118/1.4951729.

[72] E. Liakhov, O. Smolyanskaya, A. Popov, E. Odlyanitskiy, N. Balbekin, and M. Khodzitsky, "Fabrication and characterization of biotissue-mimicking phantoms in the thz frequency range", in *Journal of Physics: Conference Series*, IOP Publishing, vol. 735, 2016, p. 012 080. doi: 10.1088/1742-6596/735/1/012080.

[73] G. Menikou and C. Damianou, "Acoustic and thermal characterization of agar based phantoms used for evaluating focused ultrasound exposures", *Journal of therapeutic ultrasound*, vol. 5, pp. 1–14, 2017. doi: 10.1186/s40349-017-0093-z.

[74] J. Oudry, C. Bastard, V. Miette, R. Willinger, and L. Sandrin, "Copolymer-in-oil phantom materials for elastography", *Ultrasound in medicine & biology*, vol. 35, no. 7, pp. 1185–1197, 2009. doi: 10.1016/j.ultrasmedbio.2009.01.012.

[75] L. C. Cabrelli, F. W. Grillo, D. R. Sampaio, A. A. Carneiro, and T. Z. Pavan, "Acoustic and elastic properties of glycerol in oil-based gel phantoms", *Ultrasound in medicine & biology*, vol. 43, no. 9, pp. 2086–2094, 2017. doi: 10.1016/j.ultrasmedbio.2017.05.010.

[76] F. W. Grillo, L. C. Cabrelli, D. R. Sampaio, A. A. Carneiro, and T. Z. Pavan, "Glycerol in oil-based phantom with improved performance for photoacoustic imaging", in *2017 IEEE International Ultrasonics Symposium (IUS)*, IEEE, 2017, pp. 1–4. doi: 10.1109/ULTSYM.2017.8092278.

[77] V. Grasso, J. L. Raymond, R. Willumeit-Römer, J. Joseph, and J. Jose, "Development of a morphologically realistic mouse phantom for pre-clinical photoacoustic imaging", *Medical Physics*, vol. 50, no. 9, pp. 5757–5771, 2023. doi: 10.1002/mp.16651.

[78] G. Xu, I. A. Dar, C. Tao, X. Liu, C. X. Deng, and X. Wang, "Photoacoustic spectrum analysis for microstructure characterization in biological tissue: A feasibility study", *Applied physics letters*, vol. 101, no. 22, 2012. doi: 10.1063/1.4768703.

[79] M. Filippi, F. Garello, C. Pasquino, *et al.*, "Indocyanine green labeling for optical and photoacoustic imaging of mesenchymal stem cells after in vivo transplantation", *Journal of Biophotonics*, vol. 12, no. 5, e201800035, 2019. doi: 10.1002/jbio.201800035.

[80] V. Grasso, J. Holthof, and J. Jose, "An automatic unmixing approach to detect tissue chromophores from multispectral photoacoustic imaging", *Sensors*, vol. 20, no. 11, p. 3235, 2020. doi: 10.3390/s20113235.

[81] I. Olefir, S. Tzoumas, H. Yang, and V. Ntziachristos, "A bayesian approach to eigenspectra optoacoustic tomography", *IEEE Trans. Med. Imaging*, vol. 37, no. 9, pp. 2070–2079, 2018. doi: 10.1109/TMI.2018.2815760.

[82] L. R. Sultan, V. Grasso, J. Jose, M. Al-Hasani, M. B. Karmacharya, and C. M. Sehgal, "Advanced techniques for liver fibrosis detection: Spectral photoacoustic imaging and superpixel photoacoustic unmixing analysis for collagen tracking", *Sensors*, vol. 24, no. 14, p. 4617, 2024. doi: 10.3390/s24144617.

[83] J. Gröhl, T. Kirchner, T. J. Adler, *et al.*, "Learned spectral decoloring enables photoacoustic oximetry", *Scientific reports*, vol. 11, no. 1, p. 6565, 2021. doi: 10.1038/s41598-021-83405-8.

[84] A. Karlas, M. Kallmayer, M. Bariotakis, *et al.*, "Multispectral optoacoustic tomography of lipid and hemoglobin contrast in human carotid atherosclerosis", *Photoacoustics*, vol. 23, p. 100 283, 2021. doi: 10.1016/j.pacs.2021.100283.

[85] J. Zhang, B. Chen, M. Zhou, H. Lan, and F. Gao, "Photoacoustic image classification and segmentation of breast cancer: A feasibility study", *IEEE Access*, vol. 7, pp. 5457–5466, 2018. doi: 10.1109/ACCESS.2018.2888910.

[86] C. Shi and L. Wang, "Incorporating spatial information in spectral unmixing: A review", *Remote Sensing of Environment*, vol. 149, pp. 70–87, 2014. doi: 10.1016/j.rse.2014.03.034.

[87] S. Tzoumas, A. Nunes, N. C. Deliolanis, and V. Ntziachristos, "Effects of multispectral excitation on the sensitivity of molecular optoacoustic imaging", *Journal of Biophotonics*, vol. 8, no. 8, pp. 629–637, 2015. doi: 10.1002/jbio.201400056.

[88] D. G. Manolakis, G. A. Shaw, and N. Keshava, "Comparative analysis of hyperspectral adaptive matched filter detectors", *Proc. SPIE*, vol. 4049, pp. 2–17, 2000. doi: 10.1117/12.410332.

[89] J. Glatz, N. C. Deliolanis, A. Buehler, D. Razansky, and V. Ntziachristos, "Blind source unmixing in multi-spectral optoacoustic tomography", *Optics express*, vol. 19, no. 4, pp. 3175–3184, 2011. doi: 10.1364/OE.19.003175.

[90] N. Keshava, "A survey of spectral unmixing algorithms", *Lincoln laboratory journal*, vol. 14, no. 1, pp. 55–78, 2003.

[91] S. Tzoumas and V. Ntziachristos, "Spectral unmixing techniques for optoacoustic imaging of tissue pathophysiology", *Philosophical Transactions of the Royal Society A: Mathematical, Physical and Engineering Sciences*, vol. 375, no. 2107, p. 20 170 262, 2017. doi: 10.1098/rsta.2017.0262.

[92] Y. Wu, J. Kang, W. G. Lesniak, *et al.*, "System-level optimization in spectroscopic photoacoustic imaging of prostate cancer", *Photoacoustics*, vol. 27, p. 100 378, 2022. doi: 10.1016/j.pacs.2022.100378.

[93] S. Tzoumas, N. C. Deliolanis, S. Morscher, and V. Ntziachristos, "Unmixing molecular agents from absorbing tissue in multispectral optoacoustic tomography", *IEEE Transactions on Medical Imaging*, vol. 33, no. 1, pp. 48–60, 2013. doi: 10.1109/TMI.2013.2279994.

[94] W. F. Basener, "Clutter and anomaly removal for enhanced target detection", *Proc. SPIE*, vol. 7695, p. 769 525, 2010. doi: 10.1117/12.850303.

[95] V. Grasso, H. W. Hassan, P. Mirtaheri, R. Willumeit-Römer, and J. Jose, "Recent advances in photoacoustic blind source spectral unmixing approaches and the enhanced detection of endogenous tissue chromophores", *Frontiers in Signal Processing*, vol. 2, p. 984 901, 2022. doi: 10.3389/frsip.2022.984901.

[96] K. Maslov, H. F. Zhang, and L. V. Wang, "Effects of wavelength-dependent fluence attenuation on the noninvasive photoacoustic imaging of hemoglobin oxygen saturation in subcutaneous vasculature in vivo", *Inverse Problems*, vol. 23, no. 6, S113, 2007. doi: 10.1088/0266-5611/23/6/S09.

[97] B. T. Cox, J. G. Laufer, and P. C. Beard, "The challenges for quantitative photoacoustic imaging", *Proc. SPIE*, vol. 7177, p. 717 713, 2009. doi: 10 . 1117/12.806788.

[98] R. Hochuli, L. An, P. C. Beard, and B. T. Cox, "Estimating blood oxygenation from photoacoustic images: Can a simple linear spectroscopic inversion ever work?", *Journal of biomedical optics*, vol. 24, no. 12, pp. 121 914–121 914, 2019. doi: 10.1117/1.JBO.24.12.121914.

[99]   R. Bulsink, M. Kuniyil Ajith Singh, M. Xavierselvan, S. Mallidi, W. Steenbergen, and K. J. Francis, "Oxygen saturation imaging using led-based photoacoustic system", *Sens.*, vol. 21, no. 1, p. 283, 2021. doi: 10.3390/s21010283.

[100]   V. Grasso, R. Willumeit-Römer, and J. Jose, "Superpixel spectral unmixing framework for the volumetric assessment of tissue chromophores: A photoacoustic data-driven approach", *Photoacoustics*, vol. 26, p. 100 367, 2022. doi: 10.1016/j.pacs.2022.100367.

[101]   A. Sweeney, A. Arora, S. Edwards, and S. Mallidi, "Ultrasound-guided photoacoustic image annotation toolkit in matlab (phantom) for preclinical applications", *bioRxiv*, 2023. doi: 10.1016/j.pacs.2024.100662.

[102]   Z. Yuan, Q. Wang, and H. Jiang, "Reconstruction of optical absorption coefficient maps of heterogeneous media by photoacoustic tomography coupled with diffusion equation based regularized newton method", *Opt. Express*, vol. 15, no. 26, pp. 18 076–18 081, 2007. doi: 10.1364/OE.15.018076.

[103]   L. Zhao, M. Yang, Y. Jiang, and C. Li, "Optical fluence compensation for handheld photoacoustic probe: An in vivo human study case", *J. of Innov. Opt. Health Sci.*, vol. 10, no. 04, p. 1 740 002, 2017. doi: 10.1142/S1793545817400028.

[104]   M. N. Fadhel, E. Hysi, H. Assi, and M. C. Kolios, "Fluence-matching technique using photoacoustic radiofrequency spectra for improving estimates of oxygen saturation", *Photoacoustics*, vol. 19, p. 100 182, 2020. doi: 10.1016/j.pacs.2020.100182.

[105]   T. Kirchner, J. Gröhl, and L. Maier-Hein, "Context encoding enables machine learning-based quantitative photoacoustics", *J. Biomed. Opt.*, vol. 23, no. 5, pp. 056 008–056 008, 2018. doi: 10.1117/1.jbo.23.5.056008.

[106]   J. Gröhl, T. Kirchner, T. Adler, and L. Maier-Hein, "Estimation of blood oxygenation with learned spectral decoloring for quantitative photoacoustic imaging (lsd-qpai)", *arXiv preprint arXiv:1902.05839*, 2019. doi: 10.48550/arXiv.1902.05839.

[107]   C. Bench, A. Hauptmann, and B. Cox, "Toward accurate quantitative photoacoustic imaging: Learning vascular blood oxygen saturation in three dimensions", *J. Biomed. Opt.*, vol. 25, no. 8, pp. 085 003–085 003, 2020. doi: 10.1117/1.jbo.25.8.085003.

[108]   I. Olefir, S. Tzoumas, C. Restivo, P. Mohajerani, L. Xing, and V. Ntziachristos, "Deep learning-based spectral unmixing for optoacoustic imaging of tissue oxygen saturation", *IEEE Trans. Med. Imaging*, vol. 39, no. 11, pp. 3643–3654, 2020. doi: 10.1109/TMI.2020.3001750.

[109]   Y. Yang, S. Wang, C. Tao, X. Wang, and X. Liu, "Photoacoustic tomography of tissue subwavelength microstructure with a narrowband and low frequency system", *Applied Physics Letters*, vol. 101, no. 3, 2012. doi: 10.1063/1.4736994.

[110]   R. E. Kumon, C. X. Deng, and X. Wang, "Frequency-domain analysis of photoacoustic imaging data from prostate adenocarcinoma tumors in a murine model", *Ultrasound in medicine & Biology*, vol. 37, no. 5, pp. 834–839, 2011. doi: 10.1016/j.ultrasmedbio.2011.01.012.

[111]   S. Sinha, N. A. Rao, K. S. Valluru, B. K. Chinni, V. S. Dogra, and M. Helguera, "Frequency analysis of multispectral photoacoustic images for differentiating malignant region from normal region in excised human prostate", in *Medical Imaging 2014: Ultrasonic Imaging and Tomography*, SPIE, vol. 9040, 2014, pp. 157–165. doi: https://doi.org/10.1117/12.2043802.

[112]   X. Leng, W. Chapman Jr, B. Rao, *et al.*, "Feasibility of co-registered ultrasound and acoustic-resolution photoacoustic imaging of human colorectal cancer", *Biomedical optics express*, vol. 9, no. 11, pp. 5159–5172, 2018. doi: 10.1364/BOE.9.005159.

[113]   G. Yang, E. Amidi, W. C. Chapman Jr, *et al.*, "Co-registered photoacoustic and ultrasound imaging of human colorectal cancer", *Journal of biomedical optics*, vol. 24, no. 12, pp. 121 913–121 913, 2019. doi: 10.1117/1.JBO.24.12.121913.

[114]   E. Hysi, L. A. Wirtzfeld, J. P. May, E. Undzys, S.-D. Li, and M. C. Kolios, "Photoacoustic signal characterization of cancer treatment response: Correlation with changes in tumor oxygenation", *Photoacoustics*, vol. 5, pp. 25–35, 2017. doi: 10.1016/j.pacs.2017.03.003.

[115]   T. Erlöv, M. Cinthio, A. Edsfeldt, *et al.*, "Determining carotid plaque vulnerability using ultrasound center frequency shifts", *Atherosclerosis*, vol. 246, pp. 293–300, 2016. doi: 10.1016/j.atherosclerosis.2016.01.019.

[116]   M. Naumovska, A. Merdasa, B. Hammar, *et al.*, "Mapping the architecture of the temporal artery with photoacoustic imaging for diagnosing giant cell arteritis", *Photoacoustics*, vol. 27, p. 100 384, 2022. doi: 10.1016/j.pacs.2022.100384.

[117]   C. Kasai, K. Namekawa, A. Koyano, and R. Omoto, "Real-time two-dimensional blood flow imaging using an autocorrelation technique", *IEEE Transactions on Sonics and Ultrasonics*, vol. 32, no. 3, pp. 458–464, 1985.

[118] D. Sirmans and B. Bumgarner, "Numerical comparison of five mean frequency estimators", *Journal of Applied Meteorology and Climatology*, vol. 14, no. 6, pp. 991–1003, 1975. doi: 10.1175/1520-0450(1975)014<0991: NCOFMF>2.0.CO;2.

[119] T. Erlöv, T. Jansson, H. W. Persson, and M. Cinthio, "Scatterer size estimation using the center frequency assessed from ultrasound time domain data", *The Journal of the Acoustical Society of America*, vol. 140, no. 4, pp. 2352–2357, 2016. doi: 10.1121/1.4964107.

[120] A. B. E. Attia, S. Y. Chuah, D. Razansky, *et al.*, "Noninvasive real-time characterization of non-melanoma skin cancers with handheld optoacoustic probes", *Photoacoustics*, vol. 7, pp. 20–26, 2017. doi: https://doi.org/10.1016/j.pacs. 2017.05.003.

[121] B. Park, C. Bang, C. Lee, *et al.*, "3d wide-field multispectral photoacoustic imaging of human melanomas in vivo: A pilot study", *Journal of the European Academy of Dermatology and Venereology*, vol. 35, no. 3, pp. 669–676, 2021. doi: 10.1111/jdv.16985.